

OPTICAL- OPTICAL DOUBLE RESONANCE STUDY OF THE
3¹ A' STATE OF HCP

by

BHAVANI RAJARAM

B. Sc. Chemistry, University of Madras, India (1986)
M. Sc. Chemistry, Indian Institute of Technology, Madras, India (1988)

SUBMITTED TO THE DEPARTMENT OF CHEMISTRY
IN PARTIAL FULFILLMENT OF THE REQUIREMENTS
FOR THE DEGREE OF

DOCTOR OF PHILOSOPHY

at the

MASSACHUSETTS INSTITUTE OF TECHNOLOGY

February 1995

© Massachusetts Institute of Technology 1995
All rights reserved

Signature of Author _____

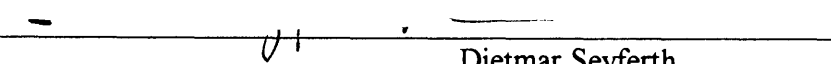
Department of Chemistry
January 4, 1995

Certified by  _____

Robert W. Field
Professor of Chemistry
thesis co-supervisor

Certified by  _____

Robert J. Silbey
Professor of Chemistry
thesis co-supervisor

Accepted by  _____

Dietmar Seyferth
Chairman, Departmental Committee on Graduate Students

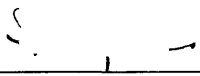
ence

MASSACHUSETTS INSTITUTE OF TECHNOLOGY

MAR 01 1995

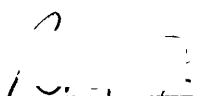
This doctoral thesis has been examined by a committee of the Department of Chemistry as follows:

Professor Sylvia T. Ceyer



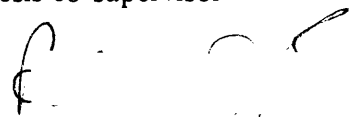
Chairman

Professor Robert W. Field




Thesis co-supervisor

Professor Robert J. Silbey



Thesis co-supervisor

Professor Robert G. Griffin



OPTICAL-OPTICAL DOUBLE RESONANCE STUDY OF THE $3^1A'$ STATE OF HCP

by

BHAVANI RAJARAM

Submitted to the Department of Chemistry
on January 4, 1995 in partial fulfillment of the requirements
for the degree of Doctor of Philosophy in Chemistry

ABSTRACT

Optical-Optical Double Resonance spectra of the vibrational levels of the $3^1A'$ state of HCP has been recorded by pumping the Q(6) rotational transition of the $(0,1^1,0)-(0,0^0,0)$ band of the $\tilde{A}^1A' \leftarrow \tilde{X}^1\Sigma^+$ electronic transition of the molecule. The corresponding spectrum of DCP (only the lowest vibrational levels) has also been recorded for the first time. Vibrational assignments that have been made imply that the molecule is quasilinear in this electronic state as suggested by *ab initio* calculations, according to which the $3^1A'$ state is the lower component of a Renner-Teller pair that correlates in the linear configuration with the $1^1\Pi$ state of the molecule. In particular, there is a rapid increase in the A rotational constant with v_2 . In addition, it appears that the bending internal coordinate plays a significant part in both modes 2 and 3, as seen by the increase in A also along the $(0,0,v_3)$ and $(0,1,v_3)$ progressions. The assigned vibrational levels have been fit to a very simple model based on the harmonic oscillator zero-order picture. However, the interpretation of the physical meaning of the resulting parameters is difficult because the vibrational potential is not well described by a Harmonic oscillator, due to the large-amplitude nature of the bending internal coordinate. Work is currently underway to apply a well established alternative model that combines Renner's matrix treatment of orbital angular momentum in linear molecules with the "bender" models capable of treating the large amplitude bending vibration. This model is known to be successful in the treatment of quasilinear molecules, by virtue of the fact that it applies equally well to linear and bent molecules.

Thesis co-supervisors: Dr. Robert W. Field Dr. Robert J. Silbey
Titles: Professors of Chemistry

Acknowledgment

I owe a great deal to many people, without whose assistance this thesis would not have been possible. First, I would like to thank Professor Field for his constant encouragement, invaluable advice, considerate help, and generous support throughout the course of this work. I am also extremely grateful to him for his kindness and support in arranging for my thesis defense to take place in Boulder (thanks to my daughter Gowri, the defense did not take place as planned).

During my first three years at MIT, I learned a great deal from David Jonas, through useful discussions and by working with him in the lab. It was on the experimental setup put together by him and Stephani Solina, that I first learned to do a double resonance experiment (SEP). This helped me immensely when I had to put together an experimental setup for my experiments. Thanks to Jianghong Wang for his help with the same.

It was a pleasure to work with Jim Lundberg for a brief while. Thanks to George Adamson, Stephani Solina, Jody Klassen, Nicole Harris, Chris Gittins, Jon O'Brien, Steve Coy, Lisa Dhar, and Zygmunt Jakubek for their friendship and their willingness to help anytime. Thanks to George Adamson for helping me to deal with the problems I faced with the old Molelectron Nd:YAG laser. Thanks to Stephani Solina for encouraging me to buy a PC, and for helping me with my limited knowledge of computers.

Thanks to Martin Mason of Princeton University for providing me with my first sample of HCP, and for generously giving me the precursor from which to synthesize DCP, that he had painstakingly synthesized. Thanks also for the many useful discussions.

My sincere thanks to Peter Giunta for his cheerful help whenever I needed it. I am extremely grateful to Bob DiGiacomo of the glass shop, and Johnny Anese and Murray Somerville of the machine shop for making whatever I required for my experiments as quickly as I needed it.

Thanks to my friends, Winnie Yip, Una Hwang, Chung-Pei Ma, Qing Feng, Li Shu, Lalitha Parameswaran, and Linda Molnar, for having made my stay at Green Hall a very pleasant experience.

Finally, I would like to thank my family for their love, encouragement, and moral support. To them, I dedicate this thesis.

TABLE OF CONTENTS

Chapter 1	Introduction		7
1.1	Spectral Manifestation of Quasilinear Behaviour	9	
	A. $^1\Sigma$ Electronic state	12	
	B. Lower Component of a Renner-Teller Split $^1\Pi$ state	18	
1.2	Notations used	23	
	References	23	
Chapter 2	Optical-Optical Double Resonance Study of the $3\ ^1A'$ State of HCP		25
2.1	Introduction	25	
2.2	Experimental	25	
	A. Sample Handling	25	
	B. OODR Apparatus	26	
	C. OODR Scheme	28	
2.3	Vibrational Assignments and Analysis	28	
	Appendix 2A	36	
	Appendix 2B	39	
	References	42	
Chapter 3	Study of the $3\ ^1A'$ State of DCP		43
3.1	Introduction	43	
3.2	Assignment of the Band Origin of the $3\ ^1A'$ State	44	
3.3	Vibrational Assignments	46	
	Appendix 3	49	
	References	50	
Chapter 4	Summary and Conclusions		51
	References	52	

Chapter 1

Introduction

This chapter serves to provide some background for the work presented in this thesis, which involves the study of the $3\ ^1A'$ state of HCP using Optical-Optical Double Resonance experiments that employ single rovibronic levels of the $\tilde{A}\ ^1A''$ state of the molecule as intermediates.

Molecules that have more than one accessible minimum in their potential energy surface in a given electronic state can vibrate with large amplitude from one conformation to another in a time scale short enough to be experimentally detectable. In the case of symmetric double minimum potentials, this is detected as tunneling doublets, and the magnitude of these splittings provide information about the barrier in the potential along a single large amplitude coordinate. In the case of the problem of the large amplitude bending of a triatomic molecule from the bent geometry to the linear geometry, because the potential has axial symmetry, the molecule in the bent configuration can rotate around its barrier to the linear configuration (there is only *one* minimum, that surrounds the barrier to linearity). In such cases, the vibration of the molecule from the bent to the linear configuration is detected as the evolution of the rotation-vibration energy level pattern from that of an asymmetric top well below the barrier maximum, to that of the linear molecule above the barrier. The work presented in this thesis involves a study of this latter problem in the $3\ ^1A'$ state of HCP.

When the molecule in the linear configuration has zero electronic orbital angular momentum ($\Lambda = 0$) about the molecular axis, this class of barrier problem is known as "*quasilinear*" [3]; whereas, if $\Lambda \neq 0$, the spectrum must be fitted to a *Renner-Teller* model [7]. When the barrier-containing vibrational mode, (the nominal bending vibration, ν_2 , in this case) can be observed systematically from $v = 0$, through pure overtone levels above the barrier maximum, an accurate characterization of the one-dimensional barrier shape can be obtained from the spectrum, provided that anharmonic interactions between the large amplitude bending vibration, and other transverse modes can be ignored.

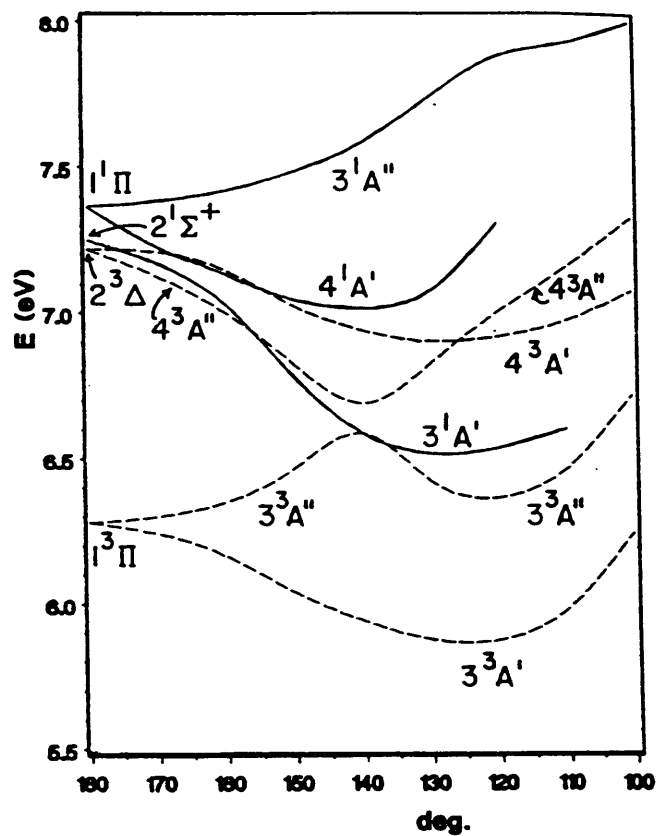


Figure 1. Energy as a function of bond angle for nonlinear HCP. Higher states. ($R_{CP} = 3.1653 a_0$, $R_{CH} = 2.0239 a_0$). (From Reference [1])

The band origin of the $3\ ^1A'$ state lies at $\sim 50642\text{ cm}^{-1}$ above the zero-point level of the ground electronic state, and the molecule has a bent equilibrium geometry in this electronic state. According to *ab initio* calculations [1], the $3\ ^1A'$ state of HCP is the lower component of a Renner-Teller pair that correlates in the linear limit, with the $n \leftarrow \pi\ 1\ ^1\Pi$ state of the molecule. In addition, these calculations also predict an avoided crossing between the $3\ ^1A'$ state and the $4\ ^1A'$ state, the latter of which correlates in the linear limit with the $\pi^{*2} \leftarrow \pi^2\ 2\ ^1\Sigma^+$ [2] state of the molecule (Figure 1).

In the adiabatic picture the top of the barrier to linearity in the $3\ ^1A'$ state lies $\sim 5900\text{ cm}^{-1}$ above the potential minimum. This energy can be easily overcome by the excitation of the bending vibration and so the molecule is expected to show quasilinear behaviour in this electronic state.

The next few paragraphs will deal with what is known about the way in which the quasilinear/Renner-Teller behaviour manifests itself in the spectrum of such a molecule.

1.1 Spectral Manifestation of quasilinear behaviour

The work that has been done by different authors on various quasilinear molecules [3-8] has demonstrated that there lies a lot of crucial information in the K_a -structure in the bending vibrational levels of such molecules¹. This is best understood by considering two specific cases: quasilinear behaviour in a) a $^1\Sigma$ electronic state, and b) the *lower* component of a Renner-Teller split $^1\Pi$ state.

¹ K_a is, in general, the quantum number for the rovibronic angular momentum and is the resultant of l , the quantum number for the vibrational angular momentum associated with the doubly-degenerate bending vibration of the molecule in the linear configuration, and Λ , which is the electronic orbital angular momentum quantum number.

$$K_a = | \Lambda + l |$$

where both Λ and l are signed quantities.

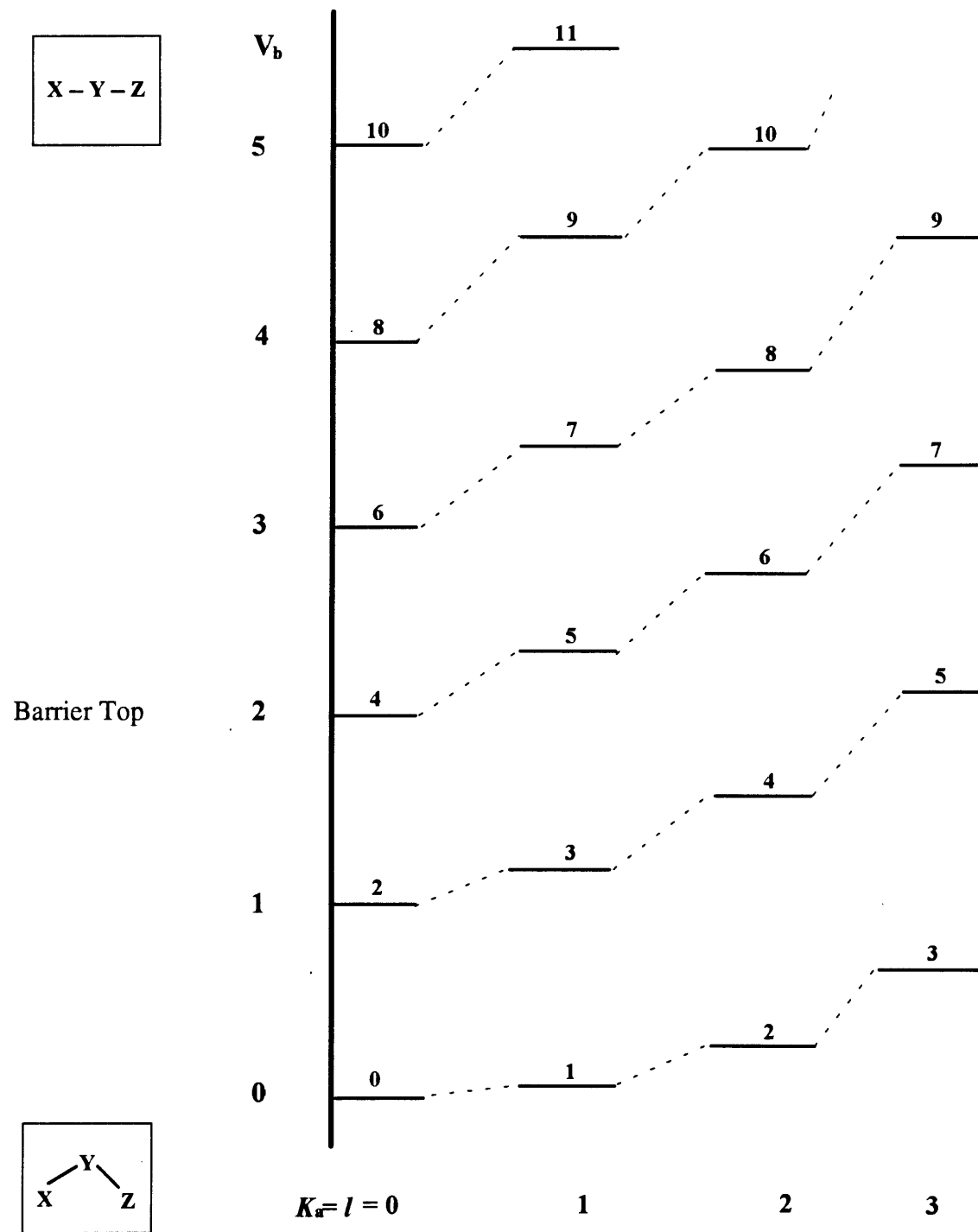


Figure 2. Vibronic energy levels of a quasilinear molecule in a $^1\Sigma$ electronic state ($\Lambda = 0, V_l = 2V_b + l$).

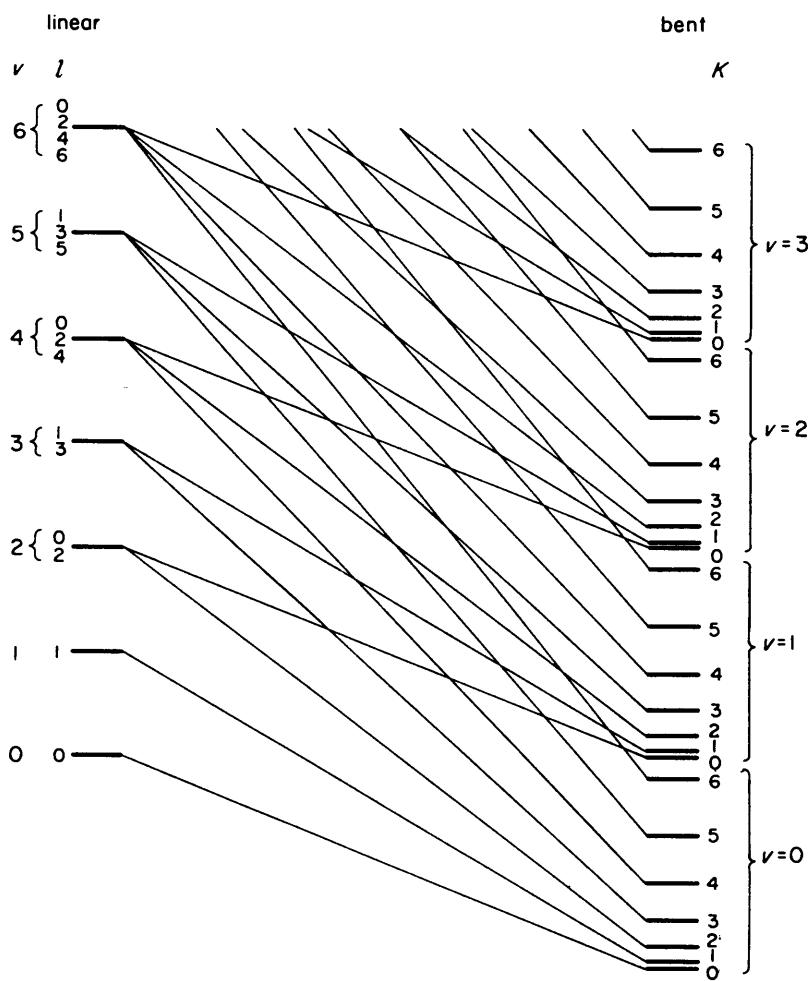


Figure 3. Correlation of the energy levels of linear and bent molecules in a non-degenerate electronic state. The height of the barrier increases from left to right; the energy curves are only qualitatively correct. From Reference [9]

A. ${}^1\Sigma$ electronic state ($\Lambda = 0, K_a = l$)

Figure 2 shows schematically, the change in the vibronic level pattern below and above the barrier to linearity (arbitrarily placed near $v_b = 2$) of a quasilinear molecule in a ${}^1\Sigma$ electronic state. v_b (v_l) refers to the number of quanta of excitation in the non-degenerate (doubly-degenerate) bending vibration of the molecule in the bent (linear) configuration. v_b and v_l are related in a ${}^1\Sigma$ electronic state through the relation:

$$v_l = 2 v_b + l .$$

This is easily seen in Figure 3, which shows the correlation of the energy levels of linear and bent molecules in a non-degenerate electronic state. Far below the barrier to linearity, the energy varies as a function of K_a , (for a particular value of v_b) roughly as $A K_a^2$, where A is the rotational constant ($\propto 1/I_a$, where I refers to the moment of inertia and 'a' is the axis of least moment of inertia). With increasing quanta in the bending vibration, there is a rapid increase in A (often referred to as $A_{0,1}$ in the later chapters to emphasize that it refers specifically to the difference in energy between the $K_a = 0$ and $K_a = 1$ sublevels with the same value of v_b), until above the barrier it becomes equal to the bending frequency of the molecule in the linear configuration. This, again, is easily seen in Figure 3, and follows from the fact that even (odd) values of l , which is equal to K_a in a ${}^1\Sigma$ electronic state, occur only for even (odd) values of v_l above the barrier. In this region, the $K_a (= l)$ sublevels that become nearly degenerate (Figure 2) are those that have the same value of v_l (the energy as a function of the vibrational angular momentum quantum number, $E(l) \cong g l^2$, where g is an anharmonicity constant for the linear molecule, and it is usually small compared to A for the molecule in the nonlinear configuration).

Quasilinear behaviour in a ${}^1\Sigma$ state was first studied by Dixon [3]. The model potential function used in this study, was a two-dimensional isotropic harmonic oscillator perturbed by a Gaussian hump:

$$V(q) = \frac{1}{2}q^2 + \alpha \exp(-\beta q^2)$$

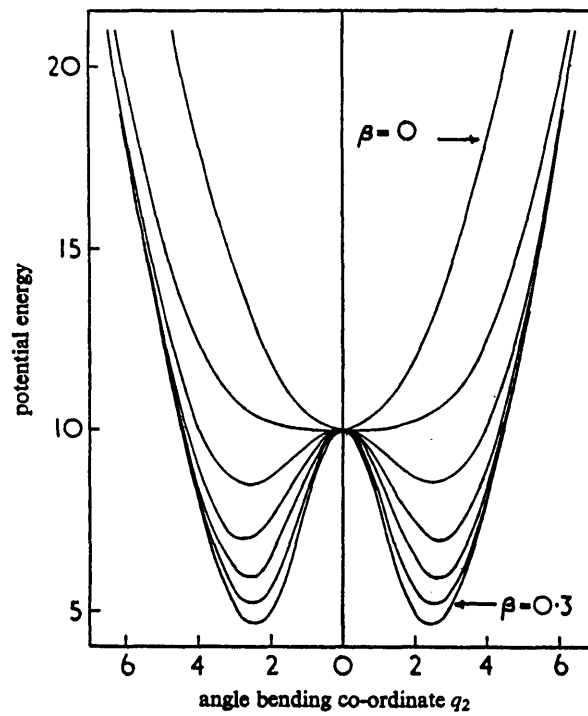


Figure 4. The potential function, $V(q) = 0.5 q^2 + \alpha \exp (-\beta q^2)$, for $\alpha = 10$ and β between 0 and 0.3, varying in steps of 0.05. From Reference [3].

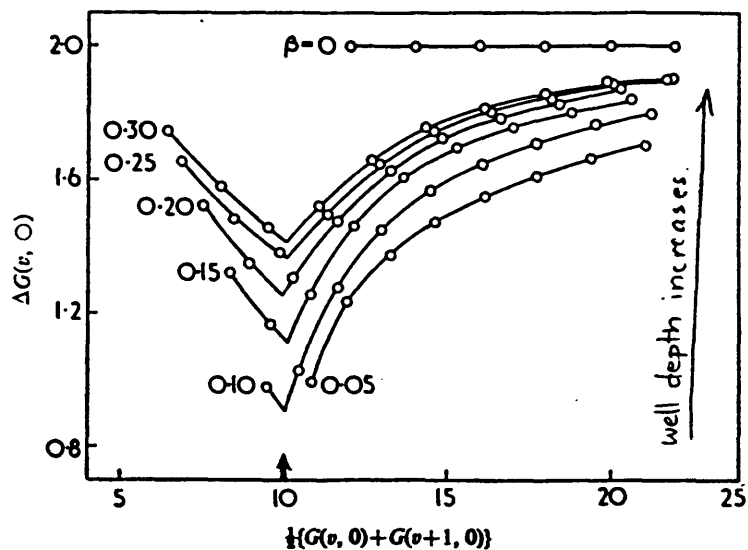


Figure 5a. The variation with total vibrational energy, of the spacing between Σ levels for $\alpha = 10$ and β between 0 and 0.30, varying in increments of 0.05. The bold arrow on the base line indicates the energy of the potential maximum. From Reference [3].

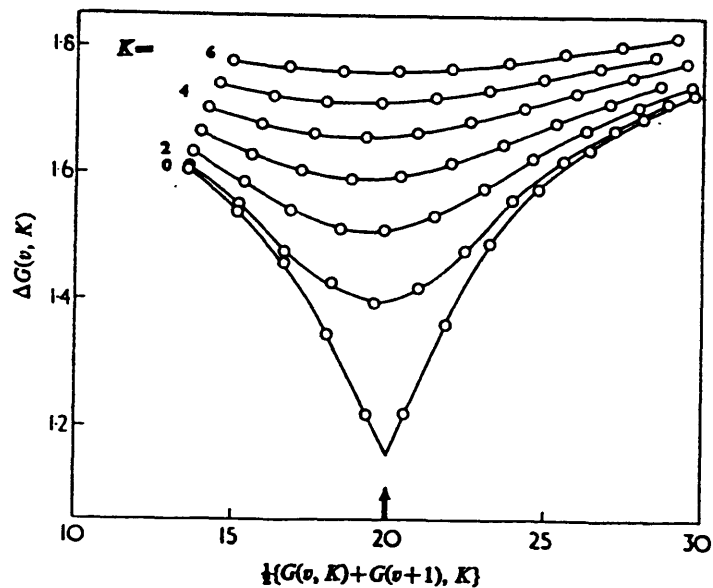


Figure 5b. The variation with K and the total vibrational energy of the vibrational spacings for $\alpha = 20$ and $\beta = 0.1$. From Reference [3].

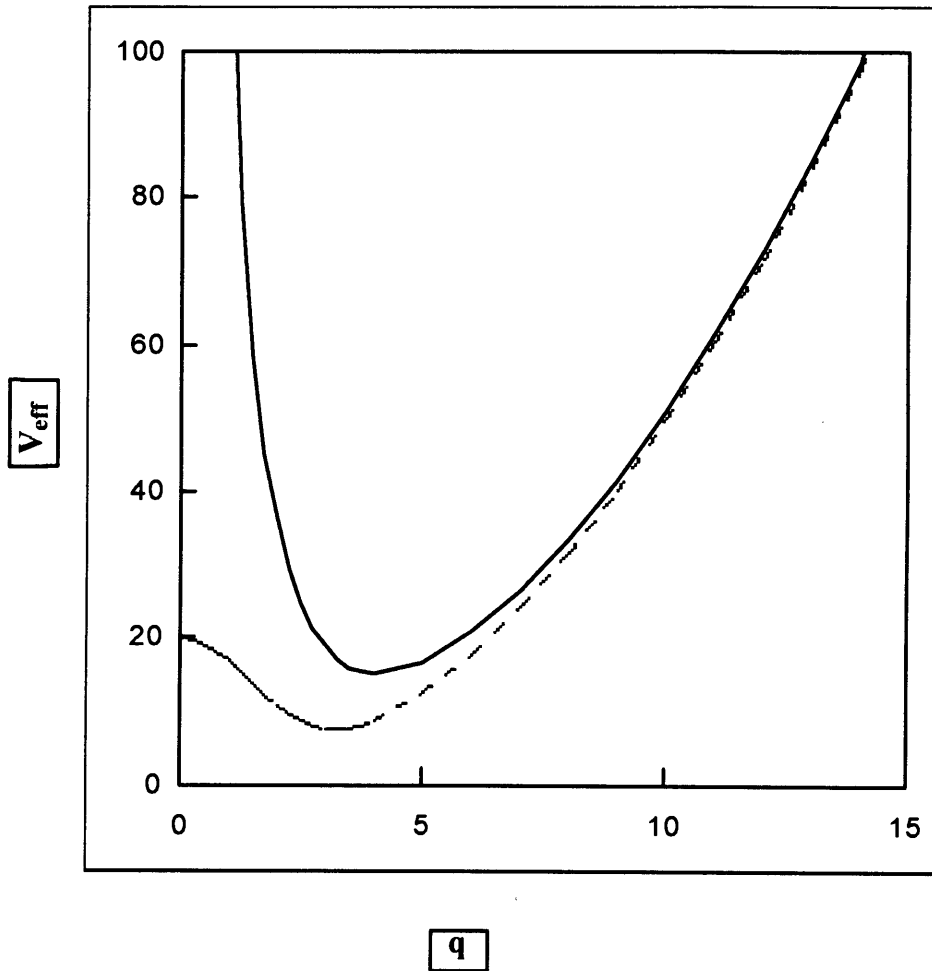


Figure 6. The effective potential, $V_{\text{eff}} = V(q) + B l^2 / q^2$, plotted as a function of q , the dimensionless bending coordinate, for $l = 0$ (dashed curve) and for l other than zero (solid curve); $\alpha = 20$, $\beta = 0.2$ and $B = 100$ were used. This figure is only qualitatively correct.

where, α and β are constants, and q is the dimensionless coordinate of the bending vibration. The shape of the above potential function is shown in Figure 4 for $\alpha = 10$, and β varying from 0 to 0.3.

The energy levels of such a system are calculated by first evaluating the matrix of the second term in the expression for $V(q)$, in a suitable finite harmonic oscillator basis set, adding this matrix to the already diagonal matrix of the two-dimensional harmonic oscillator, diagonalizing the resulting matrix, and finally multiplying the eigenvalues obtained from the diagonalization, by the bending vibrational frequency of the molecule in the linear configuration (ω_b), in order to obtain the energies in cm^{-1} units.

The matrix elements of q^2 in the two-dimensional harmonic oscillator basis are given by:

$$\langle v_t, l | q^2 | v_t, l \rangle = v_t + 1$$

$$\langle v_t - 2, l | q^2 | v_t, l \rangle = \langle v_t, l | q^2 | v_t - 2, l \rangle = -1/2 [(v_t - l)(v_t + l)]^{1/2}$$

Thus it is seen that the matrix is diagonal in l , and so a separate matrix is set up for each value of l ($= K_a$, in a $^1\Sigma$ electronic state).

The $l = K_a = 0$ sublevels of the bending vibrational levels, thus calculated for the various potential curves in Figure 4 showed that the successive vibrational intervals along the bending progression go through a minimum near the top of the barrier to linearity, for the cases where the potential has a finite hump ($\beta = 0.1$ to 0.3 , for $\alpha = 10$). This is shown in Figure 5a. For a fixed shape of the potential ($\beta = 0.1$, $\alpha = 20$), the behaviour of the vibrational intervals is shown in Figure 5b, for different values of K_a . From this figure, it is seen that the dip in the vibrational intervals is most pronounced for the $l = K_a = 0$ sublevels and it becomes less so for higher values of l . This can be understood with reference to Figure 6, where the effective potential, V_{eff} , is plotted as a function of q , for different values of l . V_{eff} can be expressed as:

$$V_{\text{eff}} = V(q) + B l^2 / q^2$$

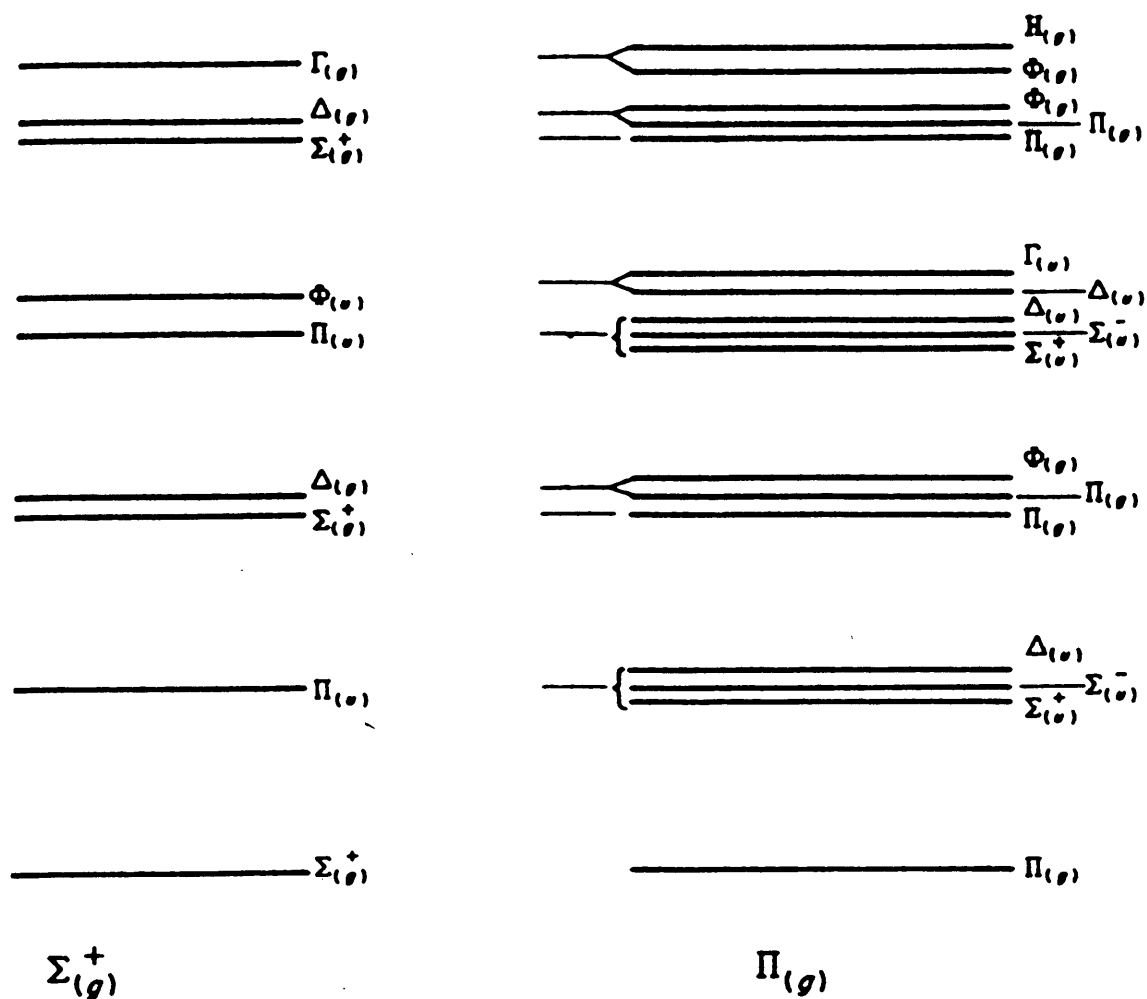


Figure 7. Vibronic species of the vibrational levels in Σ^+ , and Π electronic states of linear molecules. The subscripts g or u added in brackets give the species designation for Σ_g^+ , and Π_g electronic states of symmetrical linear molecules. From Reference [9].

where B is a constant. The second term in the above expression, represents the effect of the centrifugal force arising from the angular momentum of the nuclei around the a-inertial axis. When $l = 0$, the nuclei have zero angular momentum, and $V_{\text{eff}} = V(q)$. On the other hand, when l is non-zero, the centrifugal term gives a positive contribution to the effective potential energy, and when q is very small (that is, the nuclei are close to the linear configuration), the centrifugal term dominates over $V(q)$. Thus, the potential curves for $l = 0$ and $l \neq 0$ are qualitatively very different close to the linear geometry ($q = 0$), but similar at large q . In other words, only for $l = 0$ can the molecule actually bend through the linear geometry.

B. Lower component of a Renner-Teller split ${}^1\Pi$ state ($\Lambda = 1, K_a = |l + 1|$)

When an electronic state of the linear molecule has a finite electronic orbital angular momentum (that is, $\Lambda \neq 0$), then coupling between Λ and l is possible. This coupling, is generally called the Renner-Teller effect. In such cases only K_a , the resultant of Λ and l , is a good quantum number.

Figure 7 shows the vibronic species of the vibrational levels in a Π electronic state of a linear molecule ($K_a = 0, 1, 2, \dots$ have species $\Sigma, \Pi, \Delta, \dots$, respectively). It might be seen from this figure that there are several vibronic species (K_a values) for each bending vibrational level, v_t . Further, for each v_t , all the K_a values except one, occur in pairs, the unique value of K_a satisfying the relation, $K_a(\text{unique}) = v_t + 1$. For the K_a sublevels that occur in pairs, one has $l = K_a + \Lambda$, and the other has $l = K_a - \Lambda$. *It is the splitting between such pairs of levels, with the same value of K_a and v_t , that dominates the Renner-Teller splitting pattern.*

A simple group theoretical interpretation of the Renner-Teller effect is as follows. In the linear configuration, the molecule has axial symmetry ($C_{\infty v}$ point group, when speaking with respect to an unsymmetrical triatomic molecule), and so doubly degenerate electronic states are allowed in this geometry. However, when the molecule is bent (through the excitation of the bending vibration), the symmetry of the molecule is lowered (C_s point group, in the case of an unsymmetrical triatomic molecule), and the resulting

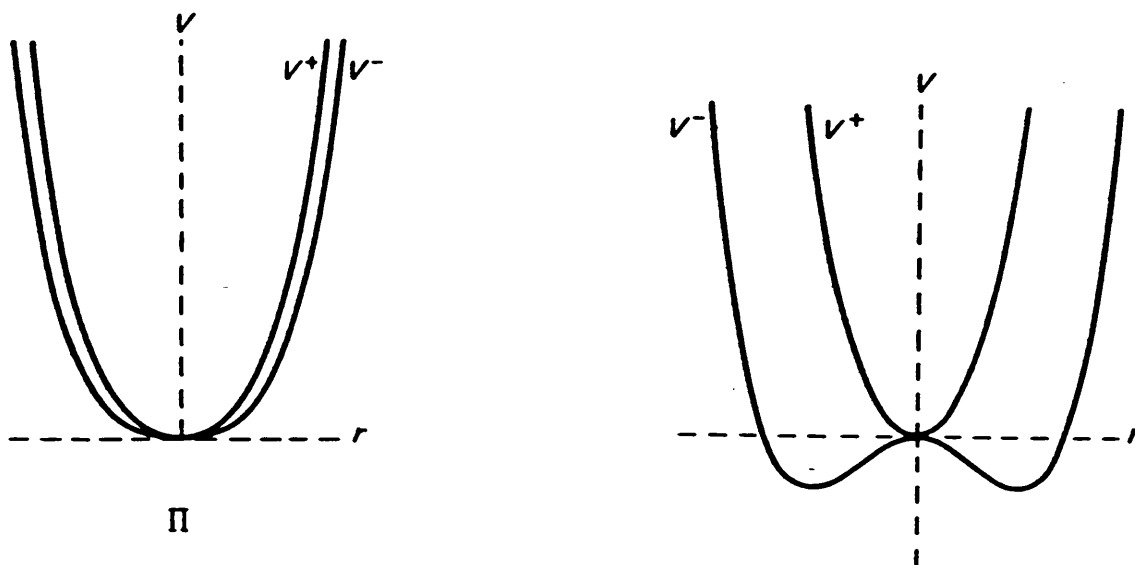


Figure 8. Potential function for the bending vibration in a Π electronic state for the cases of a) small vibronic interaction, and b) large vibronic interaction (the upper and lower components are shown as having minima in the linear and bent configurations, respectively). From Reference [9].

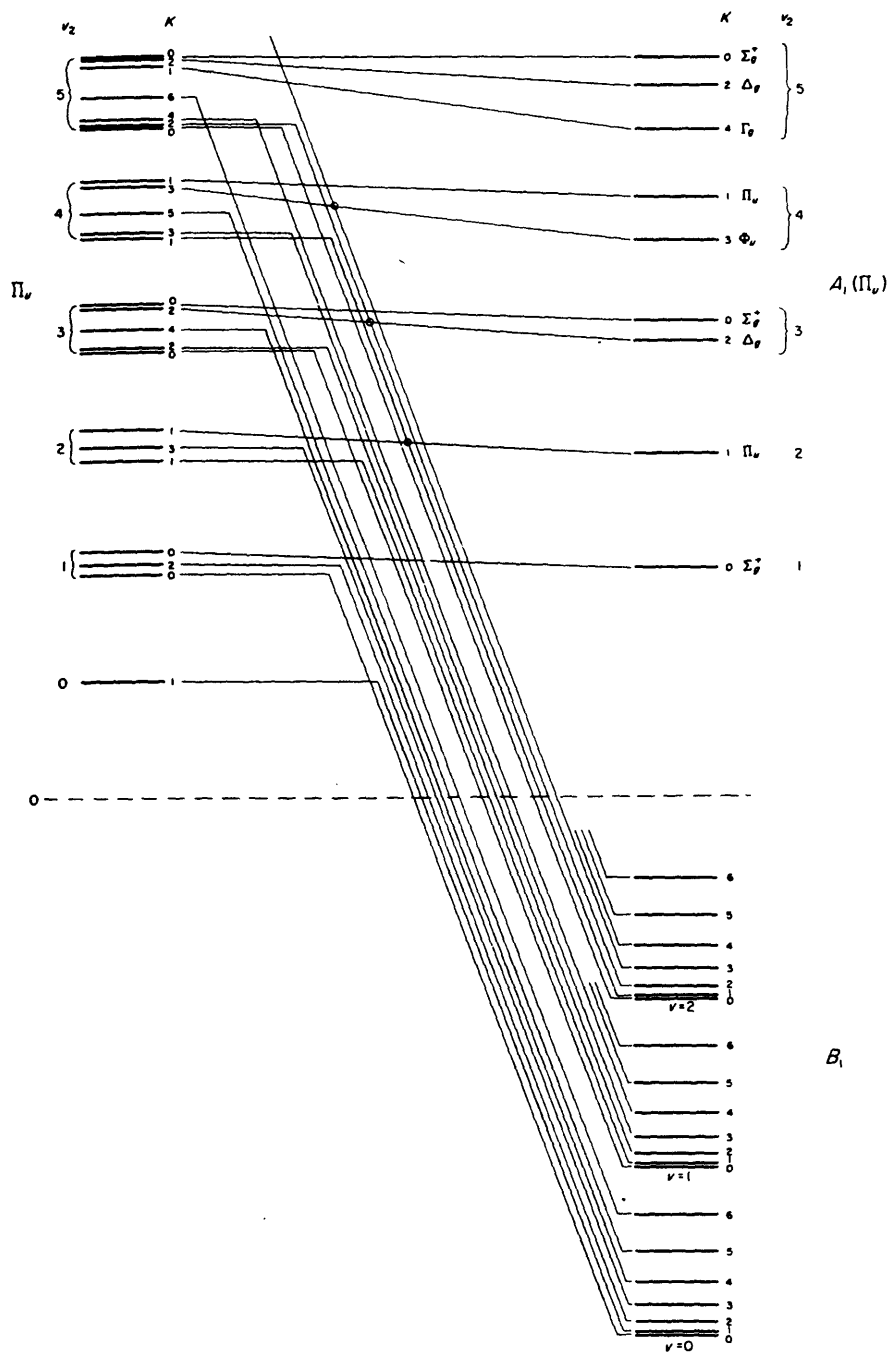


Figure 9. Correlation of vibronic levels of a Π electronic state for small and large Renner-Teller interaction. The interaction is assumed to increase from left to right. At the right, the levels correspond to b) of Figure 8. From Reference [9].

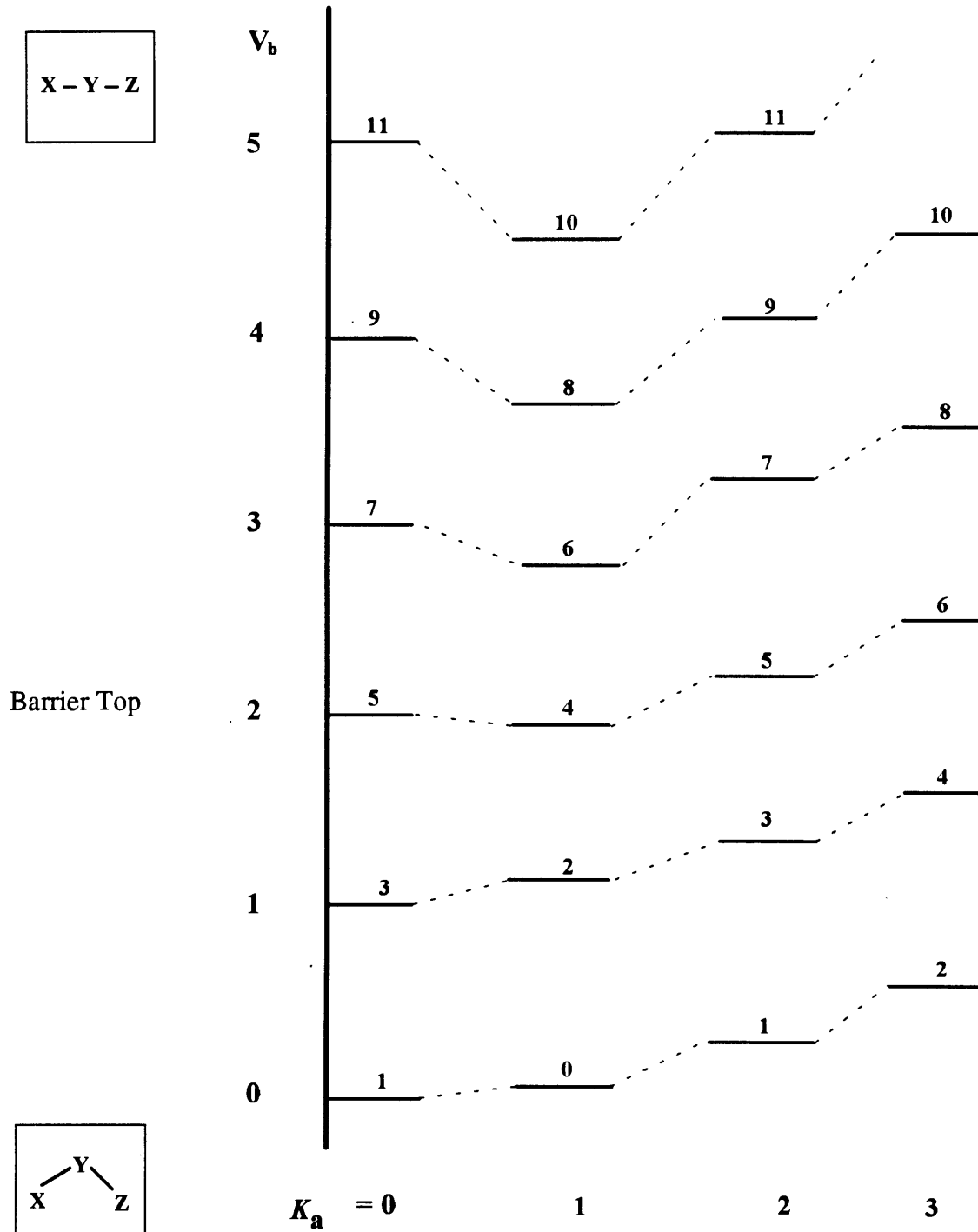


Figure 10. Vibronic energy levels of a quasilinear molecule in the *lower* Renner-Teller component of a ${}^1\Pi$ state ($\Lambda = 1$, $K_a = |l + \Lambda|$).

point group does not contain degenerate irreducible representations. Hence the double degeneracy of an electronic state in the linear configuration would be lifted when the bending vibration is excited, giving rise to two component electronic states, each of which can have a minimum in the potential energy curve, either at the linear configuration or the bent configuration (Figure 8). The correlation of the vibronic levels of a Π electronic state, for small and large Renner-Teller interaction, is shown in Figure 9.

In the case of degenerate electronic states ($\Lambda \neq 0$), the relationship between v_b and v_t is as follows :

For the sublevel with $K_a = \Lambda \pm n$ (n = positive integer),

$$v_t = 2 v_b + n$$

So, in a $^1\Pi$ state, for example, for the $K_a = 1$ ($K_a = \Lambda$ corresponds to $l = 0$ in degenerate electronic states) sublevels,

$$v_t = 2 v_b ,$$

while, for the $K_a = 0$ and $K_a = 2$ sublevels,

$$v_t = 2 v_b + 1$$

Figure 10 shows schematically, the vibronic level pattern of a quasilinear molecule in the lower component of a $^1\Pi$ state. The top of the barrier has again been placed arbitrarily close to $v_b = 2$. Here again, an initial increase in $A_{0,1}$ far below the top of the barrier is not unusual [6], but as the top of the barrier is approached, it can be seen that the $K_a = 1$ sublevel actually drops below the $K_a = 0$ sublevel. This is because, the K_a sublevel with the lowest energy for a particular value of v_t is now that with $K_a = \Lambda$, ($l = 0$), while below the barrier the lowest K_a sublevel was characterized by $K_a = 0$. Further, above the barrier to linearity, the $K_a = 0$ and $K_a = 2$ sublevels which had the same value of v_b below the barrier become nearly degenerate. Again it is seen from Figure 10 that the K_a sublevels that become nearly degenerate above the barrier are the ones that have the same value of v_t .

Thus it is seen that in the study of quasilinear molecules an investigation of the K_a -structure associated with the bending vibrational levels, especially those close to the top of the barrier, provides crucial information about the height of the barrier to linearity,

and about the orbital angular momentum of the electronic state with which the quasilinear state correlates in the linear limit. For this reason, the experiments chosen here to study the $3^1A'$ state of HCP were aimed at observing the $K_a = 0$, $K_a = 1$, and $K_a = 2$ sublevels for as many vibrational levels as possible in that electronic state. The experimental details and a vibrational analysis are presented in Chapter 2.

1.2 Notations used

Vibrational levels have been denoted as $(v_1, v_2^{K_a}, v_3)$, where v_i refers to the number of quanta of excitation in the i^{th} internal coordinate displacement. $i = 1, 2$, and 3 correspond, respectively, to the CH-stretching, the bend, and the CP-stretching internal coordinates. Footnote 1 explains the meaning of K_a .

The A rotational constant has often been denoted as $A_{0,j}$ (or as $A(0,j)$ in Figures 1, and 2 of Chapter 2) to refer specifically to the value calculated from the expression:

$$A_{0,j} = (E(K_a = j) - E(K_a = 0)) / j^2$$

\tilde{X} and \tilde{A} refer to the ground, and the first excited electronic states, respectively, single rovibronic levels of the latter of which have been chosen as intermediates in the double resonance experiments reported in this thesis.

References

1. S. P. Karna, P. J. Bruna, and F. Grein, *Can. J. Phys.*, **68**, 499 (1990).
2. J. K. Lundberg, Y. Chen, J. P. Pique, and R. W. Field, *J. Mol. Spectrosc.*, **156**, 104 (1992).
3. R. N. Dixon, *Trans. Faraday Soc.*, **60**, 1363 (1964).
4. J. W. C. Johns, *Can. J. Phys.*, **45**, 2639 (1967).
5. W. Thorson, and I. Nakagawa, *J. Chem. Phys.*, **33**, 994 (1960).

6. CH. Jungen, D. N. Malm, and A. J. Merer, *Can. J. Phys.*, **51**, 1471 (1973).
7. CH. Jungen, and A. J. Merer, *Mol. Phys.* **40**, 1 (1980).
8. CH. Jungen, K-E. J. Hallin, and A. J. Merer, *Mol. Phys.* **40**, 25 (1980).
9. G. Herzberg, *Molecular spectra and molecular structure, Vol. III - Electronic spectra and electronic structure of polyatomic molecules*. Krieger Publishing Company, Malabar, Florida, 1991.

Chapter 2

Optical-Optical Double Resonance Study of the $3^1A'$ State of HCP

2.1 Introduction

The study of the $3^1A'$ state of HCP has been aimed primarily at understanding the consequences of the quasilinear/Renner-Teller behaviour predicted for this state by *ab initio* calculations [1]. As explained in Chapter 1, the investigation of the K_a structure associated with the bending vibrational levels contains crucial information in the case of quasilinear molecules. For this reason the experiments chosen were aimed at observing the $K_a=0$, $K_a=1$, and $K_a=2$ sublevels for as many vibrational levels as possible in the $3^1A'$ state of HCP. The following sections will deal with the experimental setup, the OODR scheme, and an analysis of the observed vibrational spectrum.

2.2 Experimental

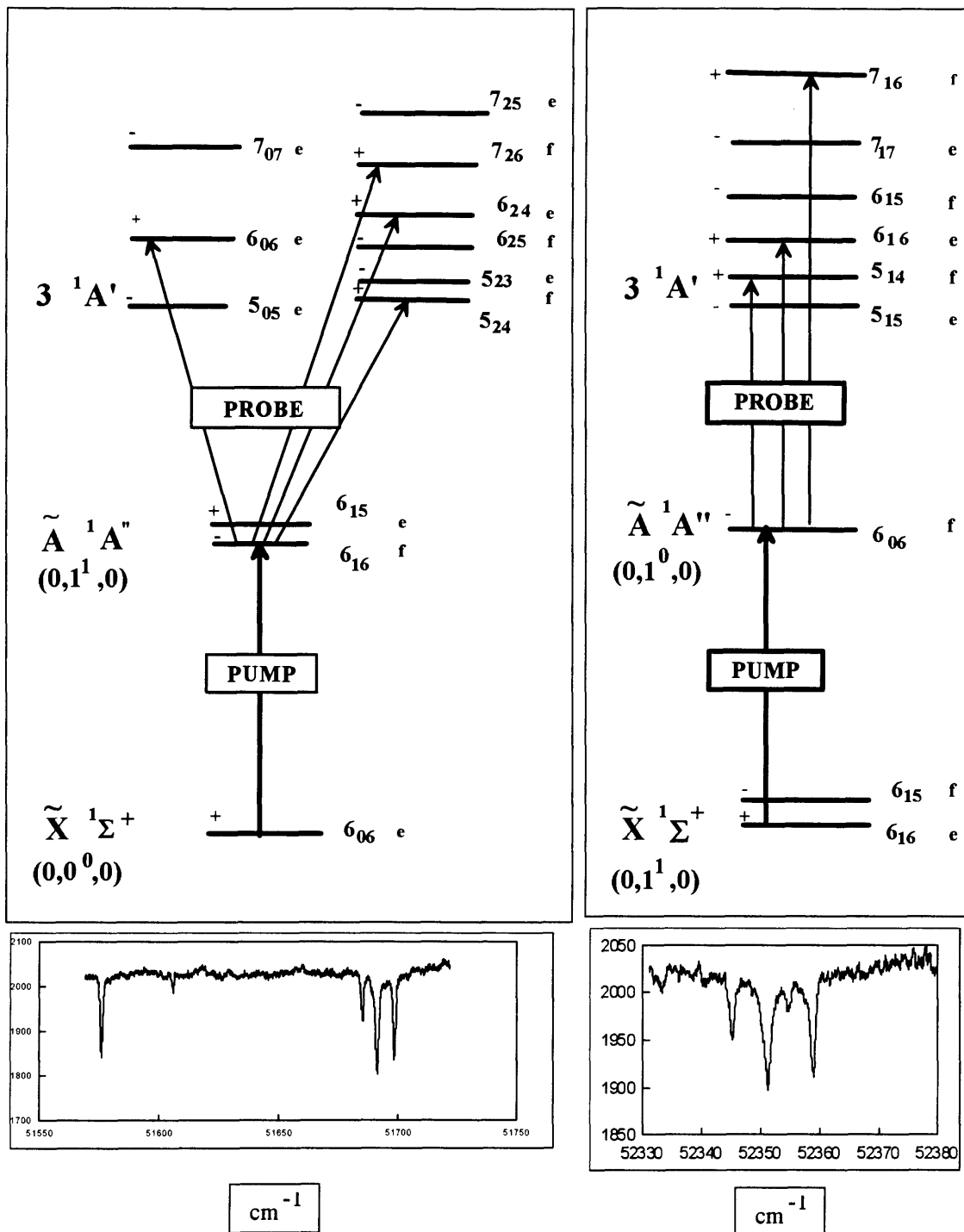
A. Sample Handling

The synthesis of HCP is described in Appendix 2B at the end of this chapter. HCP is not stable at room temperature for more than ~6 hours and so it is stored in a teflon-stoppered glass tube immersed in liquid Nitrogen. It burns in contact with air and so all sample handling such as the filling of the cell before an experiment and the pumping out of the sample at the end of the experiment have to be done using a vacuum line so as to prevent the sample from ever coming in contact with air. HCP is also known to decompose rapidly upon contact with most metals and so the use of metallic parts in the sample handling setup needs to be minimized. The 'cell' that holds the sample during the experiment is made from glass and is isolated from the rest of the sample handling system using a teflon stopper once it has been filled with the required amount of sample. The cell is filled before an experiment by subliming the desired amount of HCP (typical pressures used were ~ 400 mTorr), monitoring the pressure of the sample using a Baratron located close to the cell.

B. OODR Apparatus:

The apparatus is very similar to that used in previously reported SEP and OODR experiments [2] and hence will only be discussed briefly. The experiment basically involves the following sequence of laser excitations: 1) the frequency-doubled output (using KDP crystals) of a Nd:YAG (Molelectron MY34-20) pumped dye laser (Lambda Physik FL3002) is locked onto a single rovibronic transition of a well characterized band in the HCP $\tilde{A}^1A'' \leftarrow \tilde{X}^1\Sigma^+$ electronic transition [7]. This is called the PUMP laser and it is sent through both the arms of a two-arm glass cell using a 50/50 beam splitter. The PUMP excites fluorescence which is monitored in both arms of the cell using matched photomultiplier tubes. 2) The output of a second tunable dye laser (Lambda Physik FL3002) which is also pumped by the same Nd:YAG laser, is sent through only one of the two arms of the above mentioned cell (the 'signal' arm) in the counter-propagating direction relative to the PUMP beam. This laser is called the PROBE when it stimulates upward transitions from the PUMP-prepared intermediate state. The OODR signal is monitored as a dip in the side fluorescence excited by the PUMP laser, when the PROBE laser becomes resonant with an allowed upward transition out of the state prepared in step 1).

Depending on the HCP $\tilde{A}^1A'' \leftarrow \tilde{X}^1\Sigma^+$ band chosen in step 1), and the wavelength region desired for the PROBE, either the 532nm or the 355nm output of the Nd:YAG laser was used to pump the respective dye lasers. For most of the experiments, 7-59 filters (Corning, 3mm) were used with the photomultiplier tubes to get rid of the PUMP laser scatter. When the PROBE wavelength was close to and below 500nm, it was also found necessary to add a 7-51 (Corning, 3mm) filter to minimize scattered light due to the PROBE laser. A weak back-reflection of the PROBE beam, sent through a U/Ne hollow-cathode lamp (Starna Cells, # P886), was used for calibration of the PROBE frequency.



The rotational levels observed for the $K_a = 0$ and the $K_a = 2$ subbands of the $(0,2,0)$ vibrational level in the $3^1A'$ state of HCP.

The rotational levels observed for the $K_a = 1$ sublevel of the $(0,2,1)$ vibrational level in the $3^1A'$ state of HCP.

Figure 1. Optical-optical double resonance scheme

C. OODR Scheme:

For most of the OODR experiments the band chosen in step 1) was $\tilde{A}(0,1,0) \leftarrow \tilde{X}(0,0,0)$ (Q(6) rotational transition). The experimental data of interest, namely, the spectra of the $K_a=0$, $K_a=1$, and $K_a=2$ sublevels of the various vibrational levels of the $3^1A'$ state, had to be acquired through two separate sets of OODR experiments. Because of the $\Delta K_a = \pm 1$ selection rule applicable to each of the two steps of the double-resonance scheme, the $K_a=0$ and $K_a=2$ sublevels were accessible through the $\tilde{A}(0,1^1,0) \leftarrow \tilde{X}(0,0^0,0)$ subband, while the $K_a=1$ sublevels of the $3^1A'$ state were accessible through the $\tilde{A}(0,1^0,0) \leftarrow \tilde{X}(0,1^1,0)$ subband. Figure 1 shows both of these schemes along with the typical spectrum observed for each vibrational level in the respective schemes. All the spectra were recorded by tuning the grating; no use was made of an intracavity etalon and so the resolution is $\sim 0.5\text{cm}^{-1}$. Other vibronic bands in the $\tilde{A} \leftarrow \tilde{X}$ electronic transition were only used when searching for an expected vibrational level in the $3^1A'$ state, not observed through the $\tilde{A}(0,1,0) \leftarrow \tilde{X}(0,0,0)$ band due to an unfavourable Franck-Condon factor from the latter [see section 3.3].

2.3 Vibrational assignments and analysis:

Table A1 in the Appendix 2A at the end of this chapter lists the term values for the rotational levels of the various vibrational levels (both assigned and, as yet, unassigned) observed in the $3^1A'$ state. The assignment of the origin band was confirmed as discussed in greater detail in Chapter 3. The next higher vibrational level observed was $\sim 422\text{cm}^{-1}$ above the assigned zero-point level (ZPL). This frequency which had to correspond to a fundamental could only be assigned to that of the predominantly bending normal coordinate. The fundamental frequency of the predominantly CP-stretching normal coordinate was observed around 784cm^{-1} through the $\tilde{A}(0,0^1,0) \leftarrow \tilde{X}(0,0^0,0)$ and the $\tilde{A}(0,1^1,1) \leftarrow \tilde{X}(0,0^0,0)$ bands as well as several others (see section 3.3). At least for the lowest observed vibrational levels, it was possible to group particular $K_a=0$, $K_a=1$, and $K_a=2$ sublevels as having the same vibrational quantum numbers appropriate in the bent configuration of the molecule far below the top of the barrier to linearity. This led to the observation that the $A_{0,1}$ rotational constant, measured as $E(K_a=1) - E(K_a=0)$, varied

Table 1. Vibronic level assignments, term values, and the A rotational constants estimated both as the $K_a = 0$ - $K_a = 1$ spacing ($A_{0,1}$) and from the $K_a = 0$ - $K_a = 2$ spacing ($A_{0,2}$).

Level	Term Value (cm^{-1})			$A_{0,1}$ (cm^{-1})	$A_{0,2}$ (cm^{-1})
	$K_a = 0$	$K_a = 1$	$K_a = 2$		
(0,0,0)	50,664	50,688.3	50,758.3	24.3	23.6
(0,1,0)	51,085.8	51,112.9	51,190.9	27	26.3
(0,0,1)	51,448.5	51,474	51,550	25.5	25.4
(0,2,0)	51,576.1	51,606.3	51,691.2	30.8	28.8
(0,1,1)	51,838.4	51,874.9	51,959.6	36.6	30.3
(0,3,0)	52,073.5	52,111.5	52,209.4	38	34
(0,0,2)	52,146.8	52,176.7	52,250.3	29.9	25.9
(0,2,1)	52,306.4	52,351.2	52,454.9	44.8	37.1
(0,1,2)	52,537.5	52,580.4	52,680.6	43	35.8
(0,4,0)	52,585.6	52,635.9	-	50.3	-
(0,3,1)	52,743	52,796.2	52,887.6	53.2	36.2
(0,0,3)	52,802.2	52,849.6	-	47.5	-
(0,5,0)	52,971.9	53,050.1	53,168.9	77.3	49.2
(0,1,3)	53,199.8	53,263.2	53,343.1	63.4	35.8

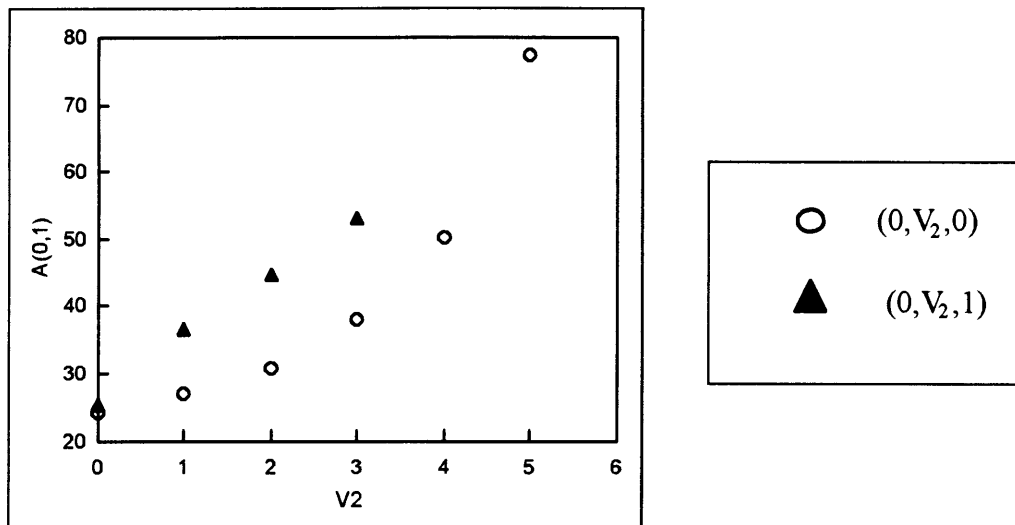


Figure 2. Variation of the A rotational constant (measured as $[E(K_a=1) - E(K_a=0)]$ in cm^{-1}) with increasing excitation in mode 2.

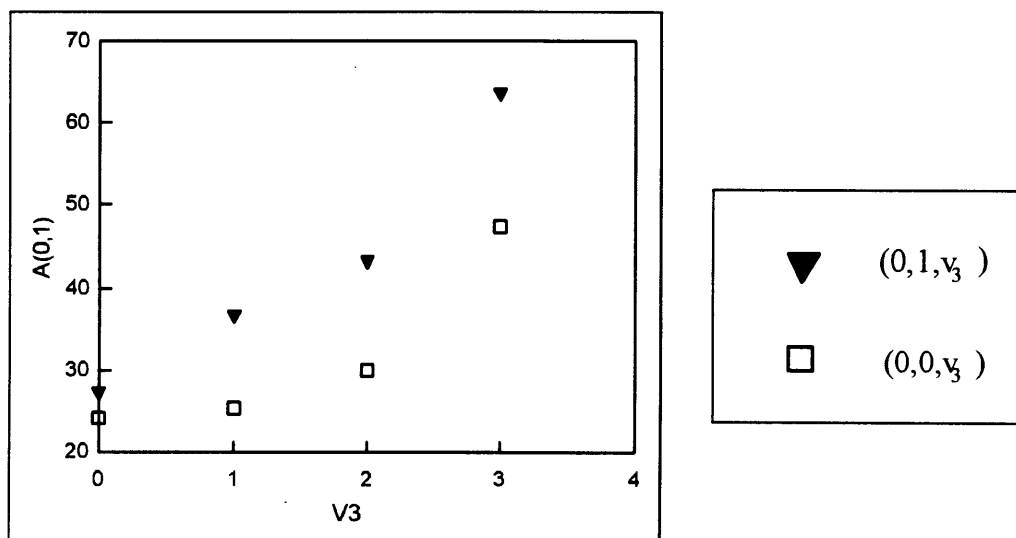


Figure 3. Variation of the A rotational constant (measured as $[E(K_a=1) - E(K_a=0)]$ in cm^{-1}) with increasing excitation in mode 3.

widely from one vibrational level to another. The vibrational assignments proposed in Table 1 were arrived at by making use of the observed fundamental frequencies and the fact that quasilinear molecules exhibit a rapid increase in the $A_{0,1}$ rotational constant with increasing excitation in the bending internal coordinate even far below the barrier to linearity. Table 2 presents the same information in the form of a Deslandres-type array and the $A_{0,1}$ values are also included in square brackets for easy reference. *It might be noted that the $A_{0,1}$ values do increase even along the $(0,0,v_3)$ and the $(0,1,v_3)$ progressions!* It does not seem possible to come up with any other more plausible assignment which would not show this dependence of the $A_{0,1}$ on v_3 . This behaviour implies a rather strong mixing between the bend, and the CP-stretching internal coordinates. Figures 2 and 3 show graphically, the variation of $A_{0,1}$ along the $(0,v_2,0)$ and $(0,v_2,1)$, and the $(0,0,v_3)$ and $(0,1,v_3)$ progressions, respectively. The $A_{0,1}$ values are always higher for the levels that have both normal modes, 2 and 3 excited, showing that both modes 2 and 3 have significant bending character. Some of the irregularities in the vibrational intervals (Table 2), especially between some of the lower members of the $(0,v_2,0)$ and $(0,v_2,1)$ progressions are likely due to Fermi-Resonance interactions involving levels such as $(0,v_2,v_3)$ and $(0,v_2+2,v_3-1)$.

Tables 3 and 4 present the results of the fits of the four progressions $(0,v_2,0)$ and $(0,v_2,1)$, and $(0,0,v_3)$ and $(0,1,v_3)$ respectively, to the expressions:

$$\begin{aligned}
 G^0(0,v_2,0) &= \omega_2^0 v_2 + x_{22}^0 v_2^2 + y_{222}^0 v_2^3 \\
 G^0(0,v_2,1) &= G^0(0,0,1) + \omega_2^{0''} v_2 + x_{22}^0 v_2^2 + y_{222}^0 v_2^3 \\
 G^0(0,0,v_3) &= \omega_3^0 v_3 + x_{33}^0 v_3^2 + y_{333}^0 v_3^3 \\
 G^0(0,1,v_3) &= G^0(0,1,0) + \omega_3^{0''} v_3 + x_{33}^0 v_3^2 + y_{333}^0 v_3^3
 \end{aligned} \tag{1}$$

where $G^0(0,v_2,v_3)$ refers to the energy above the ZPL in the $3^1A'$ state. As can be seen, the standard deviation in the residuals is fairly large and the convergence of the power series expansions is poor. The latter limits the usefulness of the model parameters in

Table 3. Results of the fits of the (0,v₂,0) and (0,v₂,1) progressions to the respective expressions in (1). The experimental uncertainty in the vibrational energies is ~2 cm⁻¹.

(0,v ₂ ,0) Progression			
<u>Parameters</u> cm ⁻¹		<u>Standard Deviation</u>	
$\bar{\omega}_2^0 = 389.3$		22 cm ⁻¹	
$x_{22}^0 = 44.9$		11 cm ⁻¹	
$y_{222}^0 = -5.9$		1 cm ⁻¹	
V ₂	EXPT. (cm ⁻¹)	CALC. (cm ⁻¹)	EXPT-CALC
1	422	428.4	-6.4
2	912	911.3	0.7
3	1,409	1,413	-4
4	1,921	1,898.1	22.9
5	2,307	2,331.1	-24.1
6	2,684	2,676.3	7.7
Standard deviation of residuals = 15.6 cm ⁻¹ .			
(0,v ₂ ,1) Progression			
<u>Parameters</u> cm ⁻¹		<u>Standard Deviation</u>	
$G^0(0, 0, 1) = 773.3$		95 cm ⁻¹	
$\bar{\omega}_2^{0''} = 366.8$		107 cm ⁻¹	
$x_{22}^0 = 41.6$		34 cm ⁻¹	
$y_{222}^0 = -5.4$		3 cm ⁻¹	
V ₂	EXPT.	CALC.	EXPT-CALC
1	1,174	1,176.4	-2.4
2	1,642	1,630.2	11.8
3	2,079	2,102.4	-23.4
4	2,584	2,560.7	23.3
5	2,961	2,972.6	-11.6
6	3,308	3,305.7	2.3

Standard deviation of residuals = 16.6 cm⁻¹.

Table 4. Results of the fits of the (0,0,v₃) and (0,1,v₃) progressions to the respective expressions in (1). The experimental uncertainty in the vibrational energies is ~2 cm⁻¹.

(0,0,v ₃) Progression			
<u>Parameters</u> cm ⁻¹		<u>Standard Deviation</u>	
$\bar{\omega}_3^0 = 796.6$		13 cm ⁻¹	
$x_{33}^0 = -32.3$		5 cm ⁻¹	
$y_{333}^0 = 2.0$		0.5 cm ⁻¹	
V ₃	EXPT. (cm ⁻¹)	CALC. (cm ⁻¹)	EXPT-CALC
1	784	766.3	17.7
2	1,483	1,480.2	2.8
3	2,138	2,153.7	-15.7
4	2,795	2,799	-4
5	3,430	3,428.3	1.7
6	4,068	4,053.8	14.2
7	4,680	4,687.7	-7.7
Standard deviation of residuals = 11.8 cm ⁻¹ .			
(0,1,v ₃) Progression			
<u>Parameters</u> cm ⁻¹		<u>Standard Deviation</u>	
$G^0(0, 1, 0) = 474.7$		40 cm ⁻¹	
$\bar{\omega}_3^{0''} = 700.7$		46 cm ⁻¹	
$x_{33}^0 = 1.1$		15 cm ⁻¹	
$y_{333}^0 = -1.5$		1 cm ⁻¹	
V ₃	EXPT.	CALC.	EXPT-CALC
1	1,174	1,174.9	-0.9
2	1,873	1,868.1	4.9
3	2,535	2,544.9	-9.9
4	3,206	3,195.9	10.1
5	3,807	3,812.1	-5.1
6	4,385	4,383.9	1.1

Standard deviation of residuals = 7.1 cm⁻¹.

predicting the positions of vibrational levels outside the range of the data used in the fits. Also, it was not possible to perform a global fit of all the assigned levels to an expression of the form:

$$G^0(0, v_2, v_3) = \omega_2^0 v_2 + x_{22}^0 v_2^2 + y_{222}^0 v_2^3 + \omega_3^0 v_3 + x_{33}^0 v_3^2 + y_{333}^0 v_3^3 + x_{23}^0 v_2 v_3 \quad (2)$$

either taking into account or not taking into account the Fermi interaction mentioned above. These difficulties have been encountered before in other molecules as well [3] and had been attributed to the inappropriate separation of the vibrational and rotational degrees of freedom in the conventional approach, on which expressions such as (1) and (2) are based. These expressions are derived from a model Hamiltonian based on a rigid-rotor, harmonic oscillator zero-order picture. Such a model is not likely to work when the vibrations cannot be regarded as being of small amplitude. The rapid increase in $A_{0,1}$ along the $(0, v_2, 0)$ progression clearly demonstrates the large amplitude nature of the bending internal coordinate in the $3^1A'$ state of HCP. Another major drawback of the conventional treatment is that it leads to a *different* rotation-vibration Hamiltonian for a linear and a non-linear molecule, while a *single* rotation-vibration Hamiltonian is required to treat a quasilinear molecule, which has a bent equilibrium geometry but which can vibrate through the linear configuration.

These difficulties have been successfully dealt with in the study of several different quasilinear molecules [4] by resorting to the more sophisticated Semi-rigid bender [5] model. Work is now in progress to try to apply this model to treat the quasilinear/Renner-Teller behaviour of HCP in the $3^1A'$ electronic state following the methods discussed in Reference [6].

Appendix 2A

Table A1. All of the rotational levels observed for the various vibronic levels of the 3¹A' state of HCP. The estimated experimental uncertainty in the energies is about 2 cm⁻¹.

$K_a = 0$		$K_a = 0$ (Cont.)		$K_a = 0$ (Cont.)	
J	Term Value (cm ⁻¹)	J	Term Value (cm ⁻¹)	J	Term Value (cm ⁻¹)
6	50,664	6	52,743	6	53,972.3
6	51,085.8	6	52,802.2	6	54,094.2
6	51,448.5	6	52,971.9	6	54,428.9
6	51,576.1	6	53,199.8	6	54,471.5
6	51,838.4	6	53,248.6	6	54,732.2
6	52,073.5	6	53,348.8	6	54,929.6
6	52,146.8	6	53,459.3	6	55,049.8
6	52,306.4	6	53,625.6	6	55,344.3
6	52,537.5	6	53,870.5	6	55,568.4
6	52,585.6	6	53,880		

$K_a = 2$

J	Parity	Term Value (cm ⁻¹)
5	f	50,751.9
6	e	50,758.3
7	f	50,765.2
5	f	51,184.1
6	e	51,190.9
7	f	51,197.4
5	f	51,543.8
6	e	51,550
7	f	51,557.1
5	f	51,685.1
6	e	51,691.2
7	f	51,698.5
5	f	51,953.1
6	e	51,959.6
7	f	51,966.8
5	f	52,203.3
6	e	52,209.4
7	f	52,216.6
5	f	52,244.1
6	e	52,250.3
7	f	52,258.1
5	f	52,448.7
6	e	52,454.9
7	f	52,462.1
5	f	52,674.4
6	e	52,680.6
7	f	52,687.9
5	f	52,881.4
6	e	52,887.6
7	f	52,895
5	f	53,162.5
6	e	53,168.9
7	f	53,176.4
6	e	53,297.5
7	f	53,304.6

 $K_a = 2$ (Cont.)

J	Parity	Term Value (cm ⁻¹)
5	f	53,336.5
6	e	53,343.1
7	f	53,350.6
5	f	53,486.2
6	e	53,492.5
7	f	53,499.6
6	e	53,847.4
7	f	53,854.4
5	f	53,931.8
6	e	53,938.2
7	f	53,945.6
5	f	54,109.1
6	e	54,113.7
7	f	54,120.7
6	e	54,485.6
7	f	54,492.8
5	f	54,716.3
6	e	54,722.5
7	f	54,729.9
5	f	55,090.9
6	e	55,097.1
7	f	55,104.4
5	f	55,521.4
6	e	55,527.8
7	f	55,534.9
5	f	55,732.7
6	e	55,739.2
7	f	55,746.8
5	f	55,824.9
6	e	55,830.6
7	f	55,837.8

 $K_a = 1$

J	Parity	Term Value (cm ⁻¹)
5	f	50,682.4
6	e	50,688.3
7	f	50,695.9
5	f	51,106.9
6	e	51,112.9
7	f	51,120.8
6	e	51,474
5	f	51,600.6
6	e	51,606.3
7	f	51,614.4
5	f	51,869.1
6	e	51,874.9
7	f	51,882.9
5	f	52,105.5
6	e	52,111.5
7	f	52,119.1
5	f	52,170.8
6	e	52,176.7
7	f	52,184.5
5	f	52,344.6
6	e	52,351.2
7	f	52,358.9
5	f	52,575.7
6	e	52,580.4
7	f	52,589.5
5	f	52,630.6
6	e	52,635.9
7	f	52,643.2
5	f	52,790.3
6	e	52,796.2
7	f	52,804
6	e	52,800.4
7	f	52,807

Table 1a. (Cont.)

$K_a = 1$ (Cont.)

J	Parity	Term Value (cm ⁻¹)
5	f	52,843.5
6	e	52,849.6
7	f	52,857.2
5	f	53,044.7
6	e	53,050.1
7	f	53,057.6
6	e	53,263.2
5	f	53,342.7
6	e	53,348.4
7	f	53,356.3
5	f	53,391.1
6	e	53,396.8
7	f	53,404.9
6	e	53,547.8
7	f	53,555.6
6	e	53,709.6
7	f	53,716.2
6	e	53,714.9
7	f	53,722.8
5	f	53,857.5
6	e	53,861.2
7	f	53,868
5	f	53,993.1
6	e	53,985.1
7	f	53,979.6
6	e	54,230.9
7	f	54,238.4
6	e	54,345.1
7	f	54,352.5
6	e	54,443.7
7	f	54,451.9
5	f	54,565.9
6	e	54,571.9
7	f	54,579.5
5	f	54,586.1
6	e	54,592
7	f	54,599.7

$K_a = 1$ (Cont.)

J	Parity	Term Value (cm ⁻¹)
5	f	54,881.6
6	e	54,887.2
7	f	54,895.1
5	f	54,962.5
6	e	54,966.9
7	f	54,972.7
5	f	55,119.1
6	e	55,124.4
7	f	55,131.9
5	f	55,167.9
6	e	55,173.1
7	f	55,180.9
5	f	55,378.5
6	e	55,383.9
7	f	55,391.6
5	f	55,507.9
6	e	55,512.4
7	f	55,520.7
5	f	55,601.4
6	e	55,607
7	f	55,614.8
6	e	55,728
7	f	55,736.4
6	e	55,755.9
7	f	55,763.8
5	f	55,767.3
6	e	55,773.6
7	f	55,781

Appendix 2B

Synthesis of HCP and DCP

HCP was synthesised by the pyrolysis of commercially available CH_3PCl_2 , using the setup shown in Figure B1. The setup consists of the following parts:

A teflon-stoppered glass tube to hold the precursor (CH_3PCl_2), a needle valve (made of Stainless steel, to resist any possible corrosion from the precursor) to control the flow of the precursor, a thermocouple gauge to monitor the pressure of the precursor in the system, a quartz tube (7mm diameter) for the pyrolysis, a cylindrical oven maintained at 900°C , using a temperature controller, two vacuum traps, one with KOH pellets and placed in a dry ice bath, and the other, placed in a liquid nitrogen bath to collect the products of the pyrolysis, a teflon-stoppered glass tube to collect and store the HCP sample, and a vacuum pump.

Prior to starting the synthesis the setup is evacuated with the oven turned on. When the pressure goes down to a few mTorr, and the temperature of the oven has stabilized close to 900°C , the dewars of the traps, 1 and 2 (Figure B1) are filled with dry ice and liquid nitrogen, respectively, and allowed to equilibrate (the vacuum pump is kept running for the entire duration of the reaction). Then the sample tube is carefully opened, and the needle valve is adjusted such that the pressure of the precursor, as measured by the thermocouple gauge placed right before the pyrolysis tube is $\sim 200\text{-}400$ mTorr.

The gaseous products of the pyrolysis first pass through the trap 1 containing KOH pellets, which removes most of the HCl formed in the reaction. Methane and other low boiling products are pumped off, while HCP and most of the other byproducts are collected in trap 2 [7]. The reaction is typically allowed to run for at least 4-5 days (replenishing the dry ice and the liquid nitrogen every 3-4 hrs.).

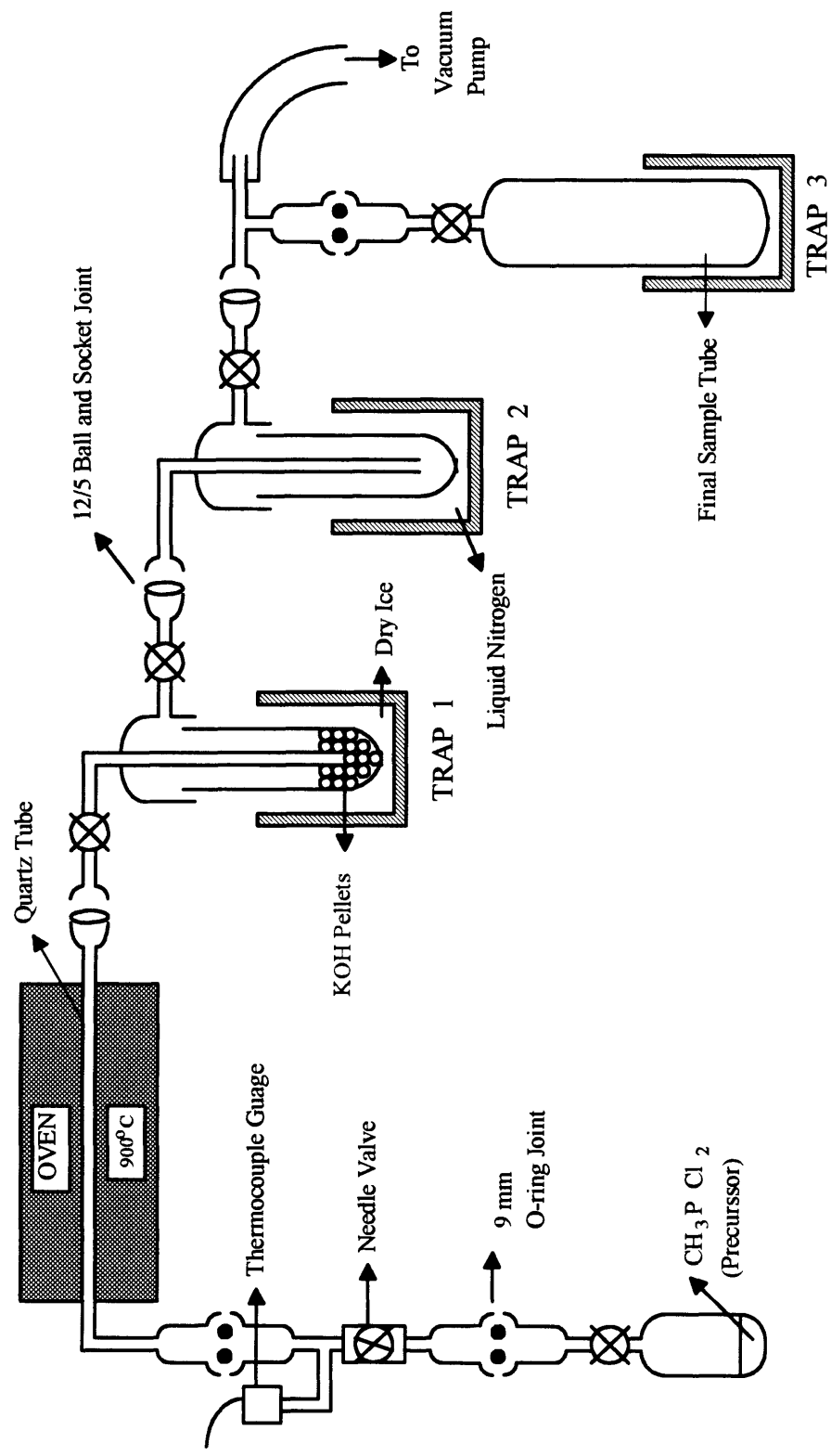
After the reaction has been stopped, HCP (along with C_2H_2 formed as a byproduct) is sublimed out of trap 2 by replacing the liquid Nitrogen with pentane slush (Pentane, cooled to its freezing point of $\sim 130^\circ\text{C}$ by slowly stirring in liquid Nitrogen) and is collected in the teflon-stoppered glass tube cooled by liquid Nitrogen in trap 3.

Synthesis of DCP:

DCP was synthesised from CDCl_2PH_2 [8], using a setup which is essentially the same as that described above for HCP. The important differences are as listed below:

- 1) Pyrolysis is carried out at a much lower temperature of $\sim 250^\circ\text{C}$.
- 2) A larger diameter ($\sim 22\text{mm}$) pyrex tubing is used for the pyrolysis.
- 3) The elimination of HCl is accomplished in the pyrolysis tube itself, by filling the tube to roughly half its diameter with anhydrous K_2CO_3 , thus making trap 1 (Figure B1) unnecessary

Figure B1. Experimental setup used for the synthesis of HCP.



References

1. S. P. Karna, P. J. Bruna, and F. Grein, *Can. J. Phys.* **68**, 499 (1990).
2. a) J. K. Lundberg, D. M. Jonas, B. Rajaram, Y. Chen, and R. W. Field, *J. Chem. Phys.* **97**, 7180 (1992).
b) C. E. Hamilton, J. L. Kinsey, and R. W. Field, *Ann. Rev. Phys. Chem.* **37**, 493 (1986).
3. F. J. Northrup, T. J. Sears, and E. A. Rohlfing, *J. Mol. Spectrosc.* **145**, 74 (1991).
4. a) Reference 3.
b) T. J. Sears, P. R. Bunker, A. R. W. McKellar, K. M. Evenson, D. A. Jennings, and J. M. Brown, *J. Chem. Phys.* **77**, 5348 (1982).
c) T. J. Sears, P. R. Bunker, and A. R. W. McKellar, *J. Chem. Phys.* **77**, 5363 (1982).
5. a) J. T. Hougen, P. R. Bunker, and J. W. C. Johns, *J. Mol. Spectrosc.* **34**, 136 (1970).
b) P. R. Bunker, and J. M. R. Stone, *J. Mol. Spectrosc.* **41**, 310 (1972).
c) P. R. Bunker, and B. M. Landsberg, *J. Mol. Spectrosc.* **67**, 374 (1977).
d) P. R. Bunker, and D. J. Howe, *J. Mol. Spectrosc.* **83**, 288 (1980).
e) P. R. Bunker, *Ann. Rev. Phys. Chem.* **34**, 59 (1983).
6. a) Ch. Jungen, and A. J. Merer, *Molecular Spectroscopy, Modern Research*, Vol. II, edited by K. Narahari Rao (Academic Press, Inc.) p.127, (1976).
b) Ch. Jungen, and A. J. Merer, *Mol. Phys.* **40**, 1 (1980).
7. J. W. C. Johns, *Can. J. Phys.*, **45**, 2639 (1967).
8. Martin A. Mason, and Kevin K. Lehmann, Private Communication.

Chapter 3

Study of the $3^1A'$ State of DCP

3.1 Introduction

The investigation of the vibrational isotope effect, resulting from the substitution of one or more atoms in a molecule with their isotopes, has been known to provide crucial information about the force field and the normal modes of vibration in a given electronic state of the molecule. The experimentally observed vibrational frequencies are generally used to determine the potential function under the influence of which the nuclei are moving in a given electronic state. However, in most cases the number of force constants, summed over all symmetry species, is larger than the $(3N-6)$ normal vibrations of an N -atomic molecule, thus the former cannot all be determined from the latter. An isotopomer has, to a very high approximation the same electronic structure. Hence, the potential function is essentially the same but the vibrational frequencies are different because of the difference in the masses. In other words, isotopic substitution does not affect the F -matrix, but alters the G -matrix [1]. So the observed vibrational frequencies of an isotopomer provide additional equations for the evaluation of the force constants. The force constants (F -matrix) are, in turn, needed to calculate the normal modes, and these are required, for example, to calculate the Franck-Condon factors for transitions between two electronic states.

Secondly, the shift in any vibrational frequency resulting from isotopic substitution enables the correlation of that vibrational frequency with a particular internal coordinate displacement. The shift in a certain vibrational frequency will be more pronounced if the atom which is replaced by its isotope has a large amplitude in that normal mode. Based on the same argument, it follows that the zero-point level in a given electronic state would show a negligible isotope shift. These aspects of isotopic substitution have made the study of the $3^1A'$ state of DCP crucial in making definitive vibrational assignments and thus better understanding the corresponding spectrum of HCP.

3.2 Assignment of the Band Origin of the $3^1A'$ State

The initial spectra of the $3^1A'$ state of HCP were recorded primarily through single rotational transitions (mostly Q(6)) in the $\tilde{A}(0,1^1,0) \leftarrow \tilde{X}(0,0^0,0)$ band. Nothing is known about the Franck-Condon factors for transitions out of the $\tilde{A}(0,1^1,0)$ level to the vibrational levels of the $3^1A'$ state, and if it was assumed that the lowest observed level in the $3^1A'$ state was indeed the zero-point level, and that all of the lowest vibrational levels up to $\sim 1650 \text{ cm}^{-1}$ had in fact been observed, then it was extremely difficult to make any plausible vibrational assignments for the observed levels. In particular, the spacing between the likely members of the pure bending progression seemed to *increase* too rapidly. So one question that definitely required an answer was, whether the lowest level observed was really the zero-point level (ZPL) of the $3^1A'$ state.

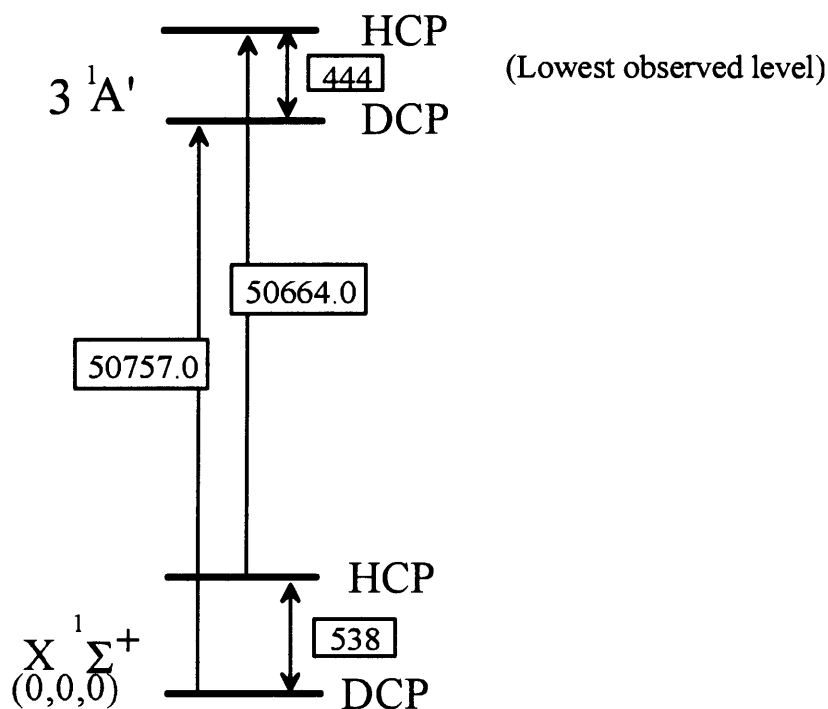


Fig 1. Relative positions of the lowest observed vibrational levels in the $3^1A'$ state of HCP and DCP (all energies are in cm^{-1}).

One way to check this was to estimate the position of the lowest observed vibrational level of the 3 ¹A' state of DCP relative to that of HCP and see whether the difference in energy seemed plausible if these levels did correspond to the ZPL's of the two isotopomers. The isotope shift in the zero-point levels can be calculated using the experimentally observed transition frequencies to the two levels under consideration, from the respective $\tilde{X}(0,0^0,0)$ levels of the two isotopomers, provided the relative positions of the $\tilde{X}(0,0^0,0)$ levels of HCP and DCP² are known (Figure 1). According to this calculation the lowest observed level in the 3 ¹A' state of DCP is about 444 cm⁻¹ lower than the corresponding level in HCP, which is in very reasonable agreement with what one would expect if these levels were in fact the respective zero-point levels of the two isotopomers.

Another way to confirm this would be to see whether the bending fundamental frequency of HCP (~ 422 cm⁻¹), arrived at by assuming that the ZPL has been assigned correctly shows the expected shift in frequency upon deuteration (this bending frequency is observed to be ~353 cm⁻¹ in the case of DCP). In the "uncoupled (vibrations) approximation"³ [2] this ratio should be equal to the ratio of the relevant diagonal G-matrix element, g_{22} . That is⁴,

$$\frac{\lambda_2'}{\lambda_2} = \frac{g_{22}'}{g_{22}} \quad (1)$$

where, the primed quantities refer to the isotopomer. In the 3 ¹A' electronic state, the right-hand side of Equation (1) works out to ~ 1.19, and the left-hand side to ~1.74. The

² This calculation is presented in the appendix to this chapter.

³ The product of all the roots λ of the secular equation $|GF-\lambda E| = 0$ is equal to the value of the determinant $|GF|$. That is,

$$\prod \lambda = |GF| = |G| |F|$$

In the "uncoupled approximation" the G and F matrices are diagonal and so it follows that,

$$\lambda_i = g_{ii} f_{ii}, \text{ or, } f_{ii} = \lambda_i / g_{ii} = 5.89146 \cdot 10^{-7} v^2 / g_{22} \quad \text{where,}$$

v is the vibrational frequency in cm⁻¹ and g_{22} is expressed in amu⁻¹.

Further, because isotopic substitution does not alter the F-matrix, we obtain Equation (1).

⁴ The g_{22} element used here is the same as the g_{33} element in section 4-6 of [1], but modified as in section 15.2 of [2] to get the units to be uniform (amu⁻¹ instead of amu⁻¹ A²)

fact that the above equation is not as accurate as one might have hoped is a reflection more of the limitations of the extreme approximations involved, rather than of an incorrect vibrational assignment. To confirm this, the same calculation was also performed for the \tilde{A} state of the molecule using the known bending fundamental frequencies [3] of HCP ($\sim 604 \text{ cm}^{-1}$) and DCP ($\sim 451 \text{ cm}^{-1}$). In that case the values obtained were 1.34 and 1.72 respectively, for the right- and left-hand sides of (1).

3.3 Vibrational Assignments

Even after the assignment of the zero-point level of the $3^1A'$ electronic state had been confirmed, vibrational assignments were not straightforward even for the lowest vibrational levels. In particular, it was not clear if the CP-stretching fundamental (ν_3) had been observed or not. Deuteration is expected to have a significant effect only on the CH-stretching frequency (ν_1 , which is not expected to be Franck-Condon active) and the bending frequency (ν_2), but not on ν_3 . The spectrum of the $3^1A'$ state of DCP, recorded through the Q(6) rotational transition of the $\tilde{A} (0,1^1,0) \leftarrow \tilde{X} (0,0^0,0)$ band, showed an extra level, not observed in the corresponding spectrum of HCP, about 708 cm^{-1} above the zero-point level. This level could be unambiguously assigned as being the (0,0,1) level based on its small A rotational constant. This identified an energy region in which to search for the ν_3 fundamental of HCP by pumping several different vibrational intermediates in the \tilde{A} electronic state, at least some of which would be expected to have a better Franck-Condon factor for access to the (0,0,1) level in the $3^1A'$ state than the intermediate level originally used ($\tilde{A} (0,1^1,0)$). Thus, the CP-stretching fundamental frequency of HCP was subsequently observed around 784 cm^{-1} above the ZPL through the $\tilde{A} (0,0^0,0)$ and $\tilde{A} (0,1^1,1)$ intermediates, among others. A list of all the levels observed in the $3^1A'$ state of DCP, with their rotational quantum number assignments, is presented in Table 1. The vibrational assignments of the observed levels, along with the A rotational constants calculated according to equation

$$A = \frac{E(K_a = 2) - E(K_a = 0)}{4} \quad (2)$$

Table 1. Energies of the rotational levels observed for the various vibronic levels in the 3 ¹A' state of DCP^a

Level (v_1, v_2, v_3)	J	K_a	Parity	Energy (cm^{-1})
(0,0,0)	6	0	e	50,757.8
	5	2	f	50,804.6
	6	2	e	50,810.1
	7	2	f	50,816.6
(0,1,0)	6	0	e	51,110.7
	5	2	f	51,163.4
	6	2	e	51,169
	7	2	f	51,175.3
(0,0,1)	6	0	e	51,466.3
	6	2	e	51,521.2
(0,2,0)	6	0	e	51,502
	5	2	f	51,559.9
	6	2	e	51,565.5
	7	2	f	51,571.9
(0,1,1)	6	0	e	51,816.7
	5	2	f	51,873.8
	6	2	e	51,879.1
	7	2	f	51,885.7
(0,0,2)	6	0	e	52,104.7
	5	2	f	52,150.3
	6	2	e	52,156.2
	7	2	f	52,162.9
(0,4,0)	6	0	e	52,188.3
	6	2	e	52,261.2
	7	2	f	52,267.4
(0,1,2)	6	0	e	52,495.3
	5	2	f	52,549.4
	6	2	e	52,555.4
	7	2	f	52,562
(0,0,3)	6	0	e	52,675.5
	5	2	f	52,720.8
	6	2	e	52,726.8
	7	2	f	52,733.5

a The experimental uncertainty in the energies presented is $\sim 2 \text{ cm}^{-1}$.

Table 2. Vibronic level assignments, term values, and estimated A rotational constants in the 3 ¹A' state of DCP^b

Level (v ₁ ,v ₂ ,v ₃)	Term Value (cm ⁻¹)		A _{0,2} ^c (cm ⁻¹)
	K=0	K=2	
(0,0,0)	50,757.8	50,810.1	13.1
(0,1,0)	51,110.7	51,169.1	14.6
(0,0,1)	51,466.3	51,521.2	13.7
(0,2,0)	51,502.1	51,565.5	15.9
(0,1,1)	51,816.7	51,879.1	15.6
(0,0,2)	52,104.7	52,156.2	12.9
(0,4,0)	52,188.3	52,261.2	18.2
(0,1,2)	52,495.3	52,555.4	15
(0,0,3)	52,675.5	52,726.8	12.8

b The experimental uncertainty in the energies presented is ~ 2cm⁻¹.

c The A rotational constant has been denoted as A_{0,2} to emphasize that it has been calculated from the K_a=2-K_a=0 spacing (Equation (2))

Table 3. Deslandres-type array for the observed vibrational levels in the 3 A' state of DCP^c

V ₂ / V ₃	0		1		2		3
0	0	708.5	708.5	638.4	1,346.9	570.8	1,917.7
	352.9		350.3		390.6		
1	352.9	705.9	1,058.8	678.7	1,737.5		
	391.3						
2	744.2						
3	-						
4	1,430.5						

c The numbers represent the *vibrational* energies in cm⁻¹.

are presented in table 2. The *vibrational* energies of the observed $K_a = 0$ sublevels are presented in the form of a Deslandres-type array in Table 3.

Appendix 3

Calculation of the difference in the ZPE of HCP and DCP in the \tilde{X} state of the molecule.

The energy of the zero-point level is given by :

$$G(0,0^0,0) = \frac{\omega_1}{2} + \omega_2 + \frac{\omega_3}{2} + \frac{x_{11}}{4} + x_{22} + \frac{x_{33}}{4} + \frac{x_{13}}{4} + \frac{x_{12}}{2} + \frac{x_{23}}{2}$$

The spectroscopic constants in the above expression for HCP and DCP, along with their sources are given in Table 1.

$$G_{\text{HCP}}(0,0^0,0) = 2985.6 \text{ cm}^{-1}$$

$$G_{\text{DCP}}(0,0^0,0) = 2447.8 \text{ cm}^{-1}$$

So, $\Delta(\text{zero-point energy}) = \underline{538 \text{ cm}^{-1}}$

Table 1. Spectroscopic constants for the ground state of HCP and DCP

HCP

$$x_{13}^b = 4.0 \text{ cm}^{-1}$$

$$x_{23}^b = 0.0 \text{ cm}^{-1}$$

$$y_{333}^0 = 2.0 \text{ cm}^{-1}$$

$$\omega_3^a = 1242.1 \text{ cm}^{-1}$$

$$\omega_3^0 = 796.6 \text{ cm}^{-1}$$

$$G^0(0, 1, 0) = 474.7 \text{ cm}^{-1}$$

$$x_{33}^b = -6.7 \text{ cm}^{-1}$$

$$x_{33}^0 = -32.3 \text{ cm}^{-1}$$

$$\omega_3^{0''} = 700.7 \text{ cm}^{-1}$$

DCP

$$x_{33}^0 = 1.1 \text{ cm}^{-1}$$

$$y_{333}^0 = -1.5 \text{ cm}^{-1}$$

a G. Strey and I. M. Mills, *Mol. Phys.* **26**, 129 (1973).

b P. Botschwina and P. Sebald, *J. Mol. Spectrosc.* **100**, 1 (1983).

c A. Cabana, Y. Doucet, J. M. Garneau, C. Pepin and P. Puget, *J. Mol. Spectrosc.* **96**, 342 (1982).

d J. Lavigne, C. Pepin and A. Cabana, *J. Mol. Spectrosc.* **104**, 49 (1984).

e J. Lavigne, C. Pepin and A. Cabana, *J. Mol. Spectrosc.* **99**, 203 (1983).

f ω_2 of DCP was calculated from the corresponding value for HCP using the Teller-Redlich product rule [4] appropriate for the Π vibration of an XYZ-type of linear molecule:

$$\frac{\omega_2^D}{\omega_2^H} = \sqrt{\frac{m_H}{m_D} \times \frac{I_x^D}{I_x^H} \times \frac{I_y^D}{I_y^H} \times \frac{M_D^2}{M_H^2}}, \quad (I_x = I_y)$$

where I_j refers to the moment of inertia about the j-inertial axis, M is the molecular weight, and m is the atomic weight of the respective isotopic species.

References

1. E. B. Wilson Jr., J. C. Decius, and P. C. Cross, *Molecular Vibrations -- The Theory of Infrared and Raman Vibrational Spectra*, McGraw-Hill, New York, 1955.
2. A. Fadini, and F. M. Schnepel, *Vibrational Spectroscopy -- Methods and Applications*, Ellis Horwood series in analytical chemistry, John Wiley and Sons, New York, 1989.
3. J. W. C. Johns, H. F. Shurvell and J. K. Tyler, *Can. J. Phys.* **47**, 893 (1969).
4. L. A. Woodward, *Introduction to the Theory of Molecular Vibrations and Vibrational Spectroscopy*, Clarendon Press, Oxford, 1972.

Chapter 4

Summary and Conclusions

The $3^1A'$ state of HCP has been studied using the Optical-Optical Double Resonance technique. The spectra show evidence for quasilinear behaviour of the molecule in this electronic state. This is seen particularly in the rapid increase in the A rotational constant (measured as $E(K_a=1) - E(K_a=0)$) with increasing quanta of excitation in the bending internal coordinate.

The OODR spectrum of the $3^1A'$ state of DCP has also been recorded for the first time. This study only included the lowest vibrational levels (up to $\sim 1900\text{ cm}^{-1}$), but it played a crucial role in the assignment of the band origin and that of the ν_3 fundamental in the $3^1A'$ state of HCP.

Vibrational assignments have been proposed, based on the observed fundamental frequencies of the two modes expected to be Franck-Condon active (ν_2 and ν_3), and the A rotational constants of the various vibrational levels, keeping in mind the fact that the A rotational constant depends on the bond angle.

The vibrational assignments led to the observation that the A rotational constant also increased along the $(0,0,\nu_3)$ and $(0,1,\nu_3)$ progressions (corresponding to increasing excitation of the nominal CP-stretching internal coordinate), suggesting that the bending internal coordinate plays a significant part in both modes 2 and 3. This involvement of the bending internal coordinate in the two modes should be borne out by a normal coordinate calculation⁵ based on the F-G matrix method [1], and would also have an important effect

⁵ If the G and F matrices are available for a molecule in the electronic state of interest, then the eigenvalues λ , of the secular equation $|GF - E\lambda| = 0$ (E is the identity matrix) give the harmonic frequencies of the vibrations. The matrix of the eigenvectors, A that diagonalize the GF matrix are related to the L-matrix, which is the transformation matrix from normal to internal coordinates (it is the inverse of this matrix that is sought).

$$\text{i.e. } S = L Q$$

on the Franck-Condon factors for transitions from the $\tilde{A} (0,1^1,0)$ intermediate to the various vibrational levels of the $3^1A'$ state. A calculation of the latter might explain the absence of levels involving excitation in mode 1 in the recorded spectra, and also the observed relative intensities of the levels with varying excitations in modes ν_2 and ν_3 .

Unfortunately, no calculations exist in the literature for the Harmonic force constants (F-matrix) in the $3^1A'$ state of the molecule. Work is now in progress to come up with the best possible guesses for the elements of the F-matrix so that the normal coordinates and hence the Franck-Condon factors for the $3^1A' \leftarrow \tilde{A} (0,1^1,0)$ transitions could be calculated.

Work is also in progress to try to model the Renner-Teller/quasilinear behaviour by fitting the assigned vibrational levels according to the methods of Reference [2], which combines Renner's matrix treatment of orbital angular momentum in linear molecules with the Bender models capable of treating large-amplitude bending motions. *This model applies equally well to linear and bent molecules*, and has been very successful also in predicting the positions of vibrational levels well outside the range of data used in the fit to the model [3].

References

1. E. B. Wilson Jr., J. C. Decius, and P. C. Cross, *Molecular Vibrations -- The Theory of Infrared and Raman Vibrational Spectra*, McGraw-Hill, New York, 1955.

where S and Q represent the set of (3N-6) internal, and normal coordinates, respectively of an N-atomic molecule. L differs from A only by a normalization factor, N.

$$\text{i.e. } L = A N$$

N is found by using the condition that L has to satisfy, namely,

$$L^T F L = \Lambda$$

$$\text{i.e., } N^2 (A^T F A) = \Lambda$$

where Λ is the diagonal matrix containing the eigenvalues. The matrix of interest is L^{-1} , which is the transformation matrix for internal to normal coordinates, and it is easily obtained by inverting L. Thus, the elements of the L^{-1} matrix would show clearly, any involvement of the bend internal coordinate that might be present in mode 3.

2. a) CH. Jungen, and A. J. Merer, *Molecular spectroscopy, Modern research*, Vol. II, edited by K. Narahari Rao (Academic Press, Inc.) p.127, (1976).
b) CH. Jungen, and A. J. Merer, *Mol. Phys.* **40**, 1 (1980).
3. a) T. J. Sears, P. R. Bunker, A. R. W. Mc Kellar, K. M. Evanson, D. A. Jennings, and J. M. Brown, *J. Chem. Phys.* **77**, 5348 (1982).
b) T. J. Sears, P. R. Bunker, and A. R. W. Mc Kellar, *J. Chem. Phys.* **77**, 5363 (1982).